AFRL-DE-PS-
TR-2006-1059

FIBER LASER ARRAYS

Thomas B. Simpson

L-3 Communications-Jaycor
3394 Carmel Mountain Road
San Diego, CA 92121

3 May 2006

Final Report

APPROVED FOR PUBLIC RELEASE; DISTRIBUTION IS UNLIMITED

AIR FORCE RESEARCH LABORATORY
Directed Energy Directorate
3550 Aberdeen Ave SE
AIR FORCE MATERIEL COMMAND
KIRTLAND AIR FORCE BASE, NM 87117-5776

DTIC COPY

Using Government drawings, specifications, or other data included in this document for any purpose other than Government procurement does not in any way obligate the U.S. Government. The fact that the Government formulated or supplied the drawings, specifications, or other data, does not license the holder or any other person or corporation; or convey any rights or permission to manufacture, use, or sell any patented invention that may relate to them.

This report has been reviewed by the Public Affairs Office and is releasable to the National Technical Information Service (NTIS). At NTIS, it will be available to the general public, including foreign nationals.

If you change your address, wish to be removed from this mailing list, or your organization no longer employs the addressee, please notify AFRL/DELO, 3550 Aberdeen Ave SE, Kirtland AFB, NM 87117-5776.

Do not return copies of this report unless contractual obligations or notice on a specific document requires its return.

This report has been approved for publication.

//SIGNED//
DR. PHILLIP PETERSON, DR-III
Project Manager

//SIGNED//
LEANNE J HENRY, Lt Col, USAF
Chief, High Power Solid State Laser Branch

//SIGNED//
L. BRUCE SIMPSON, SES
Director, Directed Energy Directorate

REPORT DOCUMENTATION PAGE

Form Approved
OMB No. 0704-0188

1. REPORT DATE *(DD-MM-YYYY)*	2. REPORT TYPE	3. DATES COVERED *(From - To)*
03-05-2006	Final Report	April 2004 – March 2006

4. TITLE AND SUBTITLE

Fiber Laser Arrays

5a. CONTRACT NUMBER
FA9451-04-C-0063

5b. GRANT NUMBER
04

5c. PROGRAM ELEMENT NUMBER
62605F

6. AUTHOR(S)
Thomas B. Simpson

5d. PROJECT NUMBER
4866

5e. TASK NUMBER
LR

5f. WORK UNIT NUMBER
02

7. PERFORMING ORGANIZATION NAME(S) AND ADDRESS(ES)

L-3 Communications - Jaycor
3394 Carmel Mountain Road
San Diego, CA 92121

8. PERFORMING ORGANIZATION REPORT NUMBER

9. SPONSORING / MONITORING AGENCY NAME(S) AND ADDRESS(ES)

Air Force Research Laboratory
3550 Aberdeen Avenue, SE
Kirtland AFB, NM 87117-5776

10. SPONSOR/MONITOR'S ACRONYM(S)

11. SPONSOR/MONITOR'S REPORT NUMBER(S)
AFRL-DE-PS-TR-2006-1059

12. DISTRIBUTION / AVAILABILITY STATEMENT

Approved for public release; distribution is unlimited.

13. SUPPLEMENTARY NOTES

The views, opinions and/or findings contained in this report are those of the author(s) and should not be construed as an official Department of the Air Force position, policy or decision, unless so designated by other documentation.

14. ABSTRACT

Experiments have been conducted to investigate the feasibility and scalability of coherent laser output from an array of fiber lasers with strong intracavity coupling. A flexible, reconfigurable experimental apparatus has been modified and configured for these investigations. Measurements taken with this apparatus during this program showed that nonlinear optical interactions in long-cavity, coherently coupled fiber laser arrays do not destroy the high efficiency coherent combining. In fact, by spreading the output power among many modes, the nonlinear optical interactions offer a path to scaling to very large arrays of length-mismatched elements. Arrays of 2-5 amplifier elements coupled using the 2 × 2 fiber couplers were constructed with emphasis on linear cavity configurations. Stimulated Brillouin Scattering and Cross Mode Coupling are identified as the key nonlinear interactions and observed distinctly using cavities with a narrow spectral bandwidth. Intracavity etaloning due to parasitic loss points at FC/APC connectors is identified as a limiting performance feature of the experimental apparatus and it is recommended that all connectorized couplings be replaced by fusion splices for future work.

15. SUBJECT TERMS

Coherent Coupling of Lasers — Erbium-doped Fiber Amplifier — Fiber Laser
Laser Array — Nonlinear Dynamics — Nonlinear Optics

16. SECURITY CLASSIFICATION OF:			17. LIMITATION OF ABSTRACT	18. NUMBER OF PAGES	19a. NAME OF RESPONSIBLE PERSON
a. REPORT	b. ABSTRACT	c. THIS PAGE			Dr. Phillip Peterson
Unclassified	Unclassified	Unclassified	Unlimited	62	19b. TELEPHONE NUMBER *(include area code)*

Standard Form 298 (Rev. 8-98)
Prescribed by ANSI Std. Z39.18

This page is intentionally left blank.

TABLE OF CONTENTS

LIST OF FIGURES

LIST OF FIGURES (continued)

LIST OF TABLES

ACKNOWLEDGEMENTS

The work and results described here have been undertaken with the ongoing collaboration of Drs. Phillip Peterson and Athanasios Gavrielides of the Air Force Research Laboratory. The author is indebted to them for their encouragement, support, insight and enthusiasm for a search for the underlying physics in a technological problem. Their parallel theoretical investigations have provided an underpinning for some of the experimental observations emphasized here. Also, the author gratefully acknowledges expert technical assistance with the experimental apparatus by Mr. Frank Doft of L-3 Communications - Jaycor.

LIST OF ACRONYMS

DFB	distributed feedback
Er	Erbium
FBG	fiber Bragg grating
MSA	microwave spectrum analyzer
RBW	resolution bandwidth
RF	radio frequency
SBS	stimulated Brillouin scattering
XMC	cross mode coupling

CONVERSION TABLE

Conversion factors for U.S. Customary to metric (SI) units of measurement.

MULTIPLY →	BY →	TO GET
TO GET ←	BY ←	DIVIDE

angstrom	1.000 000 × E −10	meter (m)
atmosphere (normal)	1.013 25 × E +2	kilo pascal (kPa)
bar	1.000 000 × E +2	kilo pascal (kPa)
barn	1.000 000 × E −28	meter^2 (m^2)
British thermal unit (thermochemical)	1.054 350 × E +3	joule (J)
calorie (thermochemical)	4.184 000	joule (J)
cal (thermochemical/cm^2)	4.184 000 × E −2	mega joule/m^2 (MJ/m^2)
curie	3.700 000 × E +1	*giga becquerel (GBq)
degree (angle)	1.745 329 × E −2	radiation (rad)
degree Fahrenheit	$t_K = (t°f + 459.67)/1.8$	degree kelvin (K)
electron volt	1.602 19 × E −19	joule (J)
erg	1.000 000 × E −7	joule (J)
erg/second	1.000 000 × E −7	watt (W)
foot	3.048 000 × E −1	meter (m)
foot-pound-force	1.355 818	joule (J)
gallon (U.S. liquid)	3.785 412 × E −3	meter^3 (m^3)
inch	2.540 000 × E −2	meter (m)
jerk	1.000 000 × E +9	joule (J)
joule/kilogram (J/kg) radiation dose absorbed)	1.000 000	Gray (Gy)
kilotons	4.183	terajoules
kip (1000 lbf)	4.448 222 × E +3	newton (N)
kip/inch^2 (ksi)	6.894 757 × E +3	kilo pascal (kPa)
ktap	1.000 000 × E +2	newton-second/m^2 (N-s/m^2)
micron	1.000 000 × E −6	meter (m)
mil	2.540 000 × E −5	meter (m)
mile (international)	1.609 344 x E +3	meter (m)
ounce	2.834 952 × E −2	kilogram (kg)
pound-force (lbs avoirdupois)	4.448 222	newton (N)
pound-force inch	1.129 848 × E −1	newton-meter (N-m)
pound-force/inch	1.751 268 × E +2	newton/meter (N/m)
pound-force/foot^2	4.788 026 × E −2	kilo pascal (kPa)
pound-force/inch^2 (psi)	6.894 757	kilo pascal (kPa)
pound-mass (lbm avoirdupois)	4.535 924 × E −1	kilogram (kg)
pound-mass-foot^2 (moment of inertia)	4.214 011 × E −2	kilogram-meter^2 (kg m^2)
pound-mass/foot^3	1.601 846 × E +1	kilogram/meter^3 (kg/m^3)
rad (radiation dose absorbed)	1.000 000 × E −2	**Gray (Gy)
roentgen	2.579 760 × E −4	coulomb/kilogram (C/kg)
shake	1.000 000 × E −8	second (s)
slug	1.459 390 × E +1	kilogram (kg)
torr (mm Hg, 0° C)	1.333 22 × E −1	kilo pascal (kPa)

* The becquerel (Bq) is the SI unit of radioactivity; 1 Bq = 1 event/s.

** The Gray (Gy) is the SI unit of absorbed radiation.

A more complete listing of conversions may be found in Metric Practice Guide E380-84, “American Society for testing and Materials.”

1.0 SUMMARY

Coherent coupling of fiber lasers has been proposed as a means to increase output beyond the capabilities of the individual lasers. It has been demonstrated that small numbers of fiber lasers, < 10, can be coherently coupled without active phase control using intracavity interferometric configurations. However, this technique is not expected to be scalable to large arrays due to the inevitability of length mismatch between laser elements of the array. Here, we demonstrate that nonlinear optical interactions lead to a spreading of the laser spectrum that can, in principal, mitigate the effects of length mismatch. To observe the nonlinear effects with modest power lasers, we use long cavity lengths, > 400 meters, to achieve a circulating power, cavity-length product greater than 100 Watt·meters.

We have identified cross mode coupling (XMC) induced by the fiber's intrinsic Kerr nonlinearity and stimulated Brillouin scattering (SBS) as the optical nonlinearities that influence the lasers at the lowest power levels. By restricting the high-reflection optical frequency band of the coherently-coupled fiber lasers, we have been able to observe the SBS separately from the XMC that leads to the spectral spreading. Because the two cannot be distinguished in coupled lasers with a larger high-reflection region, it appears that the two mechanisms are not mutually reinforcing mechanisms for broadening of the laser spectrum.

Our experimental work has been hampered by a weak feature of the experimental apparatus. The apparatus design emphasizes quick reconfiguration and uses FC/APC connectors between the various fiber elements the cavity. The connectors are readily damaged over time, even at the modest, sub-Watt, power levels that we use. This damage kept us from distinguishing whether some of the irreproducibility in our data was due to complex, nonlinear interactions as have been proposed by some, and parasitic losses due to the deteriorating fiber connectors. Therefore, we recommend a shift to fusion splices for all intracavity connections in future work.

We also propose future investigations of the use of the nonlinear-optics induced spectral broadening in combination with the use of active phase control of sub-arrays of a large array. While active control of every element of a fiber array may be prohibitively complex in a large system, control of sub-arrays that use the interferometric coherent coupling and intrinsic nonlinearities to achieve self-coherence could be a feasible solution to the coherent scaling of fiber lasers to large arrays.

2.0 INTRODUCTION

Fiber lasers have shown great promise as efficient, robust sources of coherent optical power. Several years ago, output powers from fiber lasers surpassed 100 Watts (W) and then appeared to plateau. Recently, however, the output power from individual fiber lasers has surpassed 1 kilowatt (kW) with scaling to the multi-kW range with high beam quality anticipated [1]. This improved performance has been achieved through new fabrication techniques that yield large mode area, single-transverse mode fibers. Calculations predict thermal and surface damage effects, and nonlinear optical effects such as Stimulated Brillouin Scattering (SBS) and Stimulated Raman Scattering (SRS), will limit the output from individual fiber cores to ~ 10 kW or less [1]. Peak pulse powers of ~20 kW have also been reported [2]. These lasers are based on cladding-pumped, Ytterbium-doped fiber amplifier designs with a mode area approximately an order of magnitude larger than conventional communication fibers, with the improved power scaling almost exactly with the mode area. The 20 kW peak pulse power achieved in the large area fiber, corresponding to ~2 kW in conventional fibers, is close to the limit for surface damage of 2 GW/cm^2 for fused silica. A value of 100 kW·meter (m), 10 kW·m in conventional fibers, is the calculated limit on fiber length-power product due to SRS in these lasers. Scaling to larger mode areas while limiting operation to a single confined, transverse mode becomes increasingly difficult, though there is promise in photonic crystal fibers [1].

Multiple, coherently coupled fibers have been proposed to overcome this limitation. Efficient coherent intracavity coupling with up to eight fiber lasers has been reported [3]. No active phase control has been necessary. However, calculations show that scaling to higher numbers of lasers is quickly complicated by length mismatch between the various fiber laser arms of an intracavity coupled array [4]. Length mismatch limits the high gain array modes to those that are simultaneously nearly degenerate with the modes of the individual array elements, a condition that becomes progressively harder to achieve as the number of lasers is increased. Active phase control of individual elements can compensate for length mismatch, but becomes prohibitively complex for large arrays. In this report, we will build upon our initial observation that cross mode coupling (XMC), a third order nonlinear optical process based on the fiber's intrinsic Kerr nonlinearity, of the fiber array modes leads to spectral spreading that can compensate for the narrowing effects of length mismatch for circulating power and cavity length products greater

than ~ 100 W·m for standard fibers [5]. Such power levels are readily achieved in the kilowatt single fiber lasers, even accounting for the larger mode area. Our maximum power-length product of 250 W·m is more than an order of magnitude below the ~ 10 kW·m onset for significant SRS and orders of magnitude below the intrinsic surface damage threshold limit. Based on these values, the nonlinear optical phenomena that we observe, XMC and SBS, are significant in the high power fiber lasers and will, therefore, be significant in any fiber-combining scheme to reach very high coherent power levels.

To determine the key underlying physical interactions that determine scalability and limits on the coherent combining of fiber laser arrays using intracavity coupling, we have emphasized experimental measurements using a flexible fiber array test bed. We build upon past measurements using this apparatus that have verified key aspects of the intracavity coupling. These include the observation of coherent coupling using commercial 2 x 2 fiber couplers [6], transformation of the underlying cavity modes from those of the isolated laser to a set of modes coupling all elements of the array [7], spectral broadening due to XMC [5], and here we add the observation of SBS.

We have made these observations using a flexible experimental apparatus that allows us to readily reconfigure our fiber laser arrays using standard commercial components. We have concentrated on the use of very long laser cavities, up to hundreds of meters, to increase the interaction length for nonlinear optical processes. Our progress has been slowed by the recurring observation of parasitic intracavity losses at the connection points of the various components of our cavities. These parasitic losses have had strong effects on the spectrum of the coherent output and kept us from isolating characteristics that occur from intrinsic cavity and nonlinear coupling effects with those due to the parasitic reflections. To date, we have used FC/APC connectors and we have now enough experience to recommend that these connectors be removed from the cavities for future work. Commercially available devices are now available at a reasonable cost that will allow us to make repeatable low-loss, low back-scatter fusion splices of the single-mode fiber that we use. Further, low-cost, in-line fiber components are now commercially available that allow precise phase control of the intra-cavity optical field [8].

In this report, we first review some key results from the last program made using a unidirectional ring laser configuration with four coupled amplifiers, and then present new results made using

linear configuration with four and five coupled amplifiers. We will then describe measurements made to investigate intracavity etaloning. While constructive interference is the key to the coherent combining of coupled cavities, unwanted etaloning is observed to, at the very least, hide the underlying intrinsic spectral characteristics of the coupled array. Next, we move on to a new, two-laser configuration that emphasized operation with the cavity restricted to lase over a narrow spectral range by proper choice of fiber Bragg gratings (FBGs). This configuration yielded what was perhaps the key finding of the current program, the unambiguous observation of SBS in the long cavities. We then present results on relaxation pulsations in restricted wavelength lasers. We conclude with a discussion of the relation of this work to other results presented recently, and recommendations for future work.

3.0 REVIEW OF THE UNIDIRECTIONAL RING LASER CAVITY

The current effort is the third in a series of contracts investigating coherent intracavity coupling of fiber laser arrays. The first, Contract No. F296001-00-C-0001, helped to initiate some of the enthusiasm in this field by first demonstrating that coherent intracavity coupling could be achieved with commercially available 2 x 2 fiber couplers being developed for the communications industry [6,9], without the need for active cavity phase control. The second, Contract No. F29601-01-C-0223, demonstrated that the intracavity coupling led to the creation of new set of array modes that were not simply a combination of the modes of the individual lasers but had a mode spacing that reflected the overall array characteristics [5,7]. However, only those array modes that were simultaneously degenerate with a mode of each of the individual array elements would experience large gain and significant coherent output. The verification of the linear analyses of arrays in this work and others [3] led to the conclusion that arrays with only linear intracavity coupling could not be scaled to large numbers due to inevitable cavity-length mismatch [4]. Therefore we inaugurated the investigation of nonlinear optical properties to overcome this limitation [5]. A unidirectional, ring-laser configuration was chosen so that spatial hole burning of the gain medium, and the potential for nonlinearities based on this, would not have to be considered.

For the investigations of a unidirectional ring-laser cavity, provision was made for arrays of from two to five amplifier elements. Figures 1 and 2 are schematics of the ring laser configuration built around the independent Er-doped fiber amplifiers. Figure 1 shows a single amplifier configuration that highlights the common loop components of the ring configuration and the diagnostics. The laser power circulates clockwise in the ring due to the directional character of the intracavity optical circulator and optical isolator. The fiber polarizer forces oscillation on one polarization axis only and the polarization rotator compensates for any polarization rotation in the ring. The FBG defines a narrow spectral band, typically ~ 30-50 gigahertz (GHz) with our units, where the cavity round trip losses are minimized. Extra lengths of fiber can be added in different sections of the ring. Because there is about 5-dB loss through the optical circulator, adding the fiber after the circulator rather than before puts a lower intensity beam through any extra fiber in the common path. Adding between the FBG and the circulator causes twice the path length change for a given length of fiber plus the fact that there is now the potential for nonlinear interaction of the counter-propagating beams in a long segment. We increased the

cavity length by up to 400 m of fiber, an 800-m path length change when the extra fiber is added between the FBG and the circulator. Light is coupled out of the ring at a fiber coupler. We typically use 10% output coupling though 50% and 90% are readily accommodated. The output light is directed to photodiodes whose temporal output is monitored using oscilloscopes and spectral output is monitored with a MSA. The output can also be mixed with a single-frequency distributed feedback (DFB) semiconductor laser that is used as an optical local oscillator to generate optical spectra. The temperature of the DFB laser is varied so that its frequency is swept across the high-reflection band of the FBG. A sweep takes about 10 s, so that second and sub-second fluctuations in the optical spectra cannot be followed.

Scaling to more than one amplifier is accomplished within the box marked Amplifier Segment in Figure 1 and shown schematically in Figure 2. The two-amplifier configuration, Figure 15(a) uses 50/50 fiber couplers to split and remix the optical beams. A second polarization rotator is needed in one leg to correct for the fact that each amplifier may induce a different polarization shift. Alternatively, moving the rotator from the common path segment to the amplifier arm to match the components in the two arms creates a more symmetric configuration. Extra fiber can be added in either arm to vary the length mismatch. We used patchchords of 1 m and multiples, with some shorter length path variation possible with the repositioning of the fiber polarizers, i.e., moving the polarization rotator in the common leg to the amplifier arm that contains no rotator. We will return to this configuration later, when we are discussing amplitude pulsations in coherently coupled cavities. Similar considerations apply for the four-amplifier configuration shown in Figure 2(b) which we emphasize now. The 2×2 coupler (chains) contain output ports that can be monitored to observe the coherent combining. When coherence is maximized output at these points is minimized.

Figure 3 shows a relatively low-resolution optical spectrum for a four-amplifier configuration with a long cavity. The laser output is compared with the transmission spectrum of the FBG. The optical spectrum and the measurement of the transmitted signal through the grating are generated with the use of a DFB laser diode that has its temperature swept to change its output optical frequency. The DFB laser acts as the local oscillator for a heterodyne measurement to generate the optical spectrum. The optical spectrum consists of a periodic set of peaks with a spacing of ~ 2.3 GHz confined to the high reflection band of the FBG. This fairly closely corresponds to the

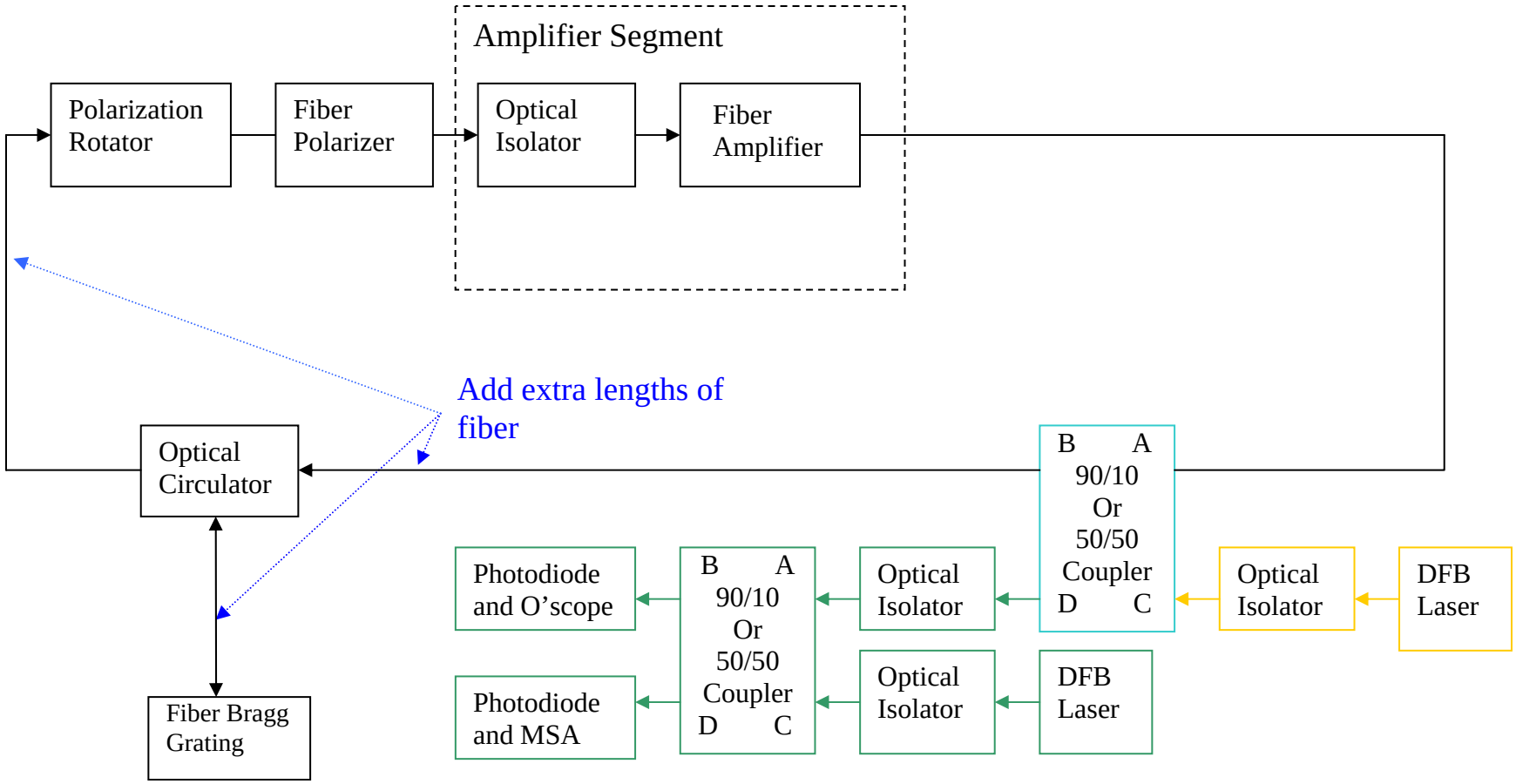

Figure 1. **Schematic of the flexible experimental apparatus in a unidirectional ring configuration. Shown here is the configuration with a single amplifier. The 90/10 or 50/50 coupler with the light blue outline is the cavity output coupler. The elements outlined in green are the output diagnostics path with the DFB laser here used as a local oscillator to generate optical spectra with the photodiode and MSA. The other DFB laser is used to inject a single frequency optical signal into the cavity. Extra lengths of single mode fiber can be added to the cavity. The difference between adding the extra fiber before or after the optical circulator is the reduced circulating power after the circulator. Adding the fiber between the circulator and the FBG doubles the optical path for a given fiber length and adds the path where there are counter propagating beams. The optical circulator and the optical isolators enforce unidirectional optical beam circulation within the cavity.**

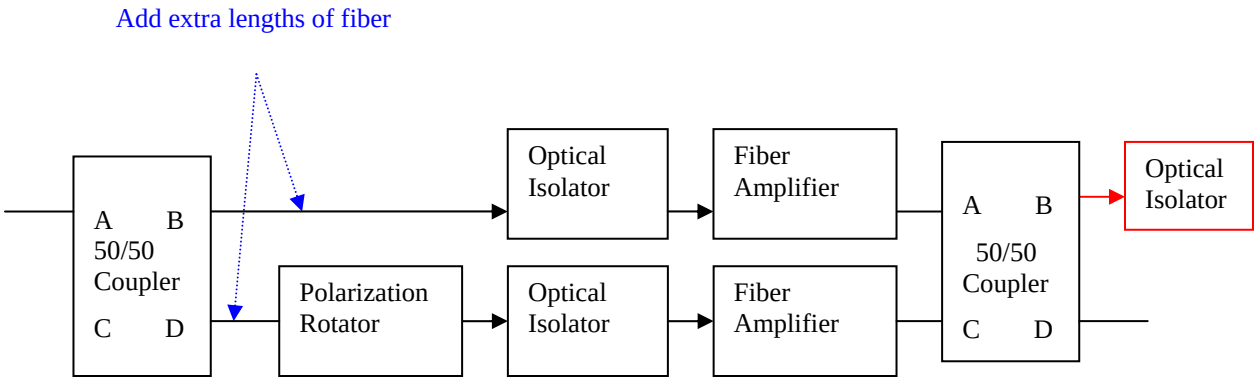

Figure 2(a). Schematic of the two-amplifier segment.

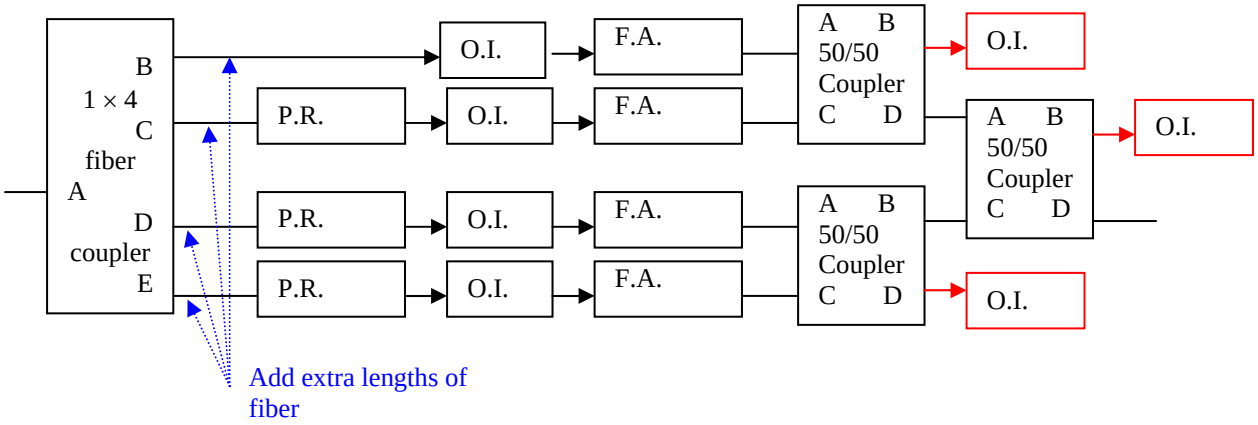

Figure 2(b). Schematic of the four-amplifier segment.

Figure 2. Schematic of the amplifier segments for the multilaser configurations. The optical isolators marked in red at the outputs of the 2 (a) and 4 (b) amplifier segments are the loss ports minimized by coherence that can be monitored with photodetectors. The input and output lines fit into the connections at the edges of the dashed box labeled Amplifier Segment in Figure 1. Extra lengths of fiber can be added to vary the length mismatch in the various arms of the array. P.R. = Polarization rotator, O.I. = Optical Isolator, F.A. = Fiber Amplifier

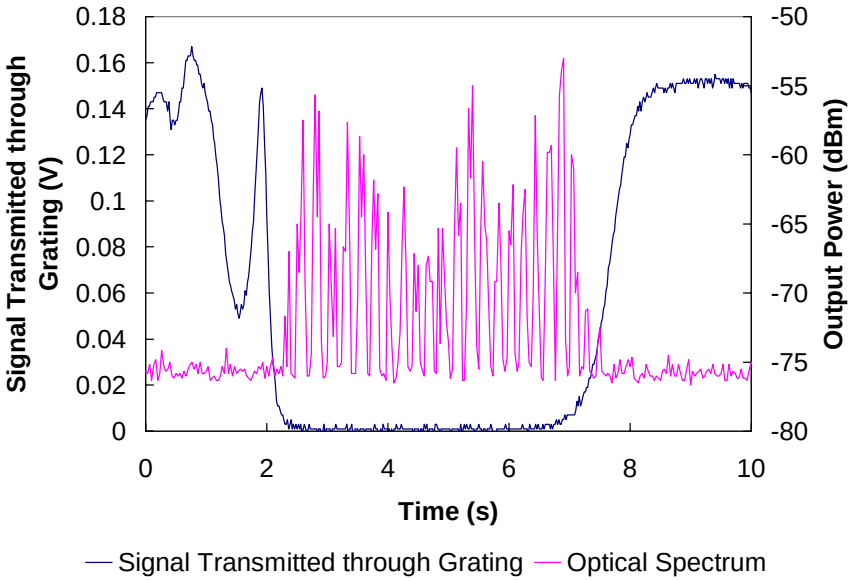

Figure 3. The optical spectrum is superposed on the transmission spectrum of the FBG that defines the bandwidth of the ring cavity. The smallest length mismatch corresponds to a frequency spacing of ~2.3 GHz. The conversion from time of the frequency sweep to frequency is 1 s ~10 GHz (though not quite linear across sweep).

shortest length mismatch between the amplifier paths. This dense set of peaks is in stark contrast to a sparse and irregular set of peaks observed with the shorter, 10-50 m, cavity length.

To verify that length mismatch produced the spacing, we used or ability to reconfigure the apparatus to further shorten the smallest amplifier path length mismatch. Figure 4 shows the resulting optical spectrum. Now the separation is ~ 4.8 GHz. The 2.3 GHz and 4.8 GHz frequency offsets are the highest frequencies expected to be generated in the respective spectra based on the length mismatches. Each peak in the spectra varied apparently randomly in time.

Because of their low resolution, the optical spectra did not yield much detail. To observe greater spectral detail, we observed the output power spectra from the photodetector. Figure 5 shows the broadband power spectrum for the laser configuration corresponding to Figure 3. The features separated by 2.3 GHz are seen to be made up of a dense set of features that, in Figure 6, are shown to have dominant spacings of ~200 megahertz (MHz) and ~40 MHz, corresponding to the ~1-m and ~5-m length mismatches between different amplifier paths. Each of these peaks is further shown to be made up of a dense set of lines offset by the 0.24-MHz cavity mode frequency spacing (see Figure 7). These mode peaks also have structure, as shown in Figure 8.

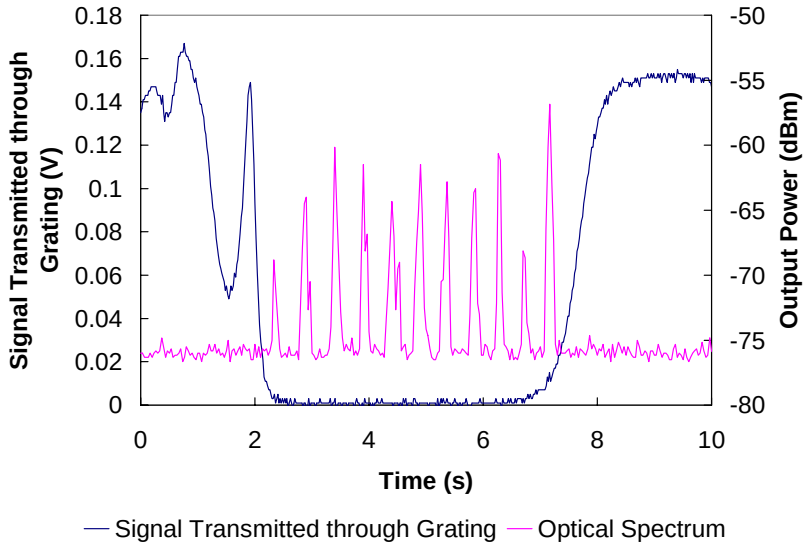

Figure 4. Optical spectrum using the smallest cavity length mismatch. The optical spectrum is superposed on the transmission spectrum of the FBG that defines the bandwidth of the ring cavity. The smallest length mismatch corresponds to a frequency spacing of ~4.8 GHz. The conversion from time of the frequency sweep to frequency is 1 s ~10 GHz (though not quite linear across sweep).

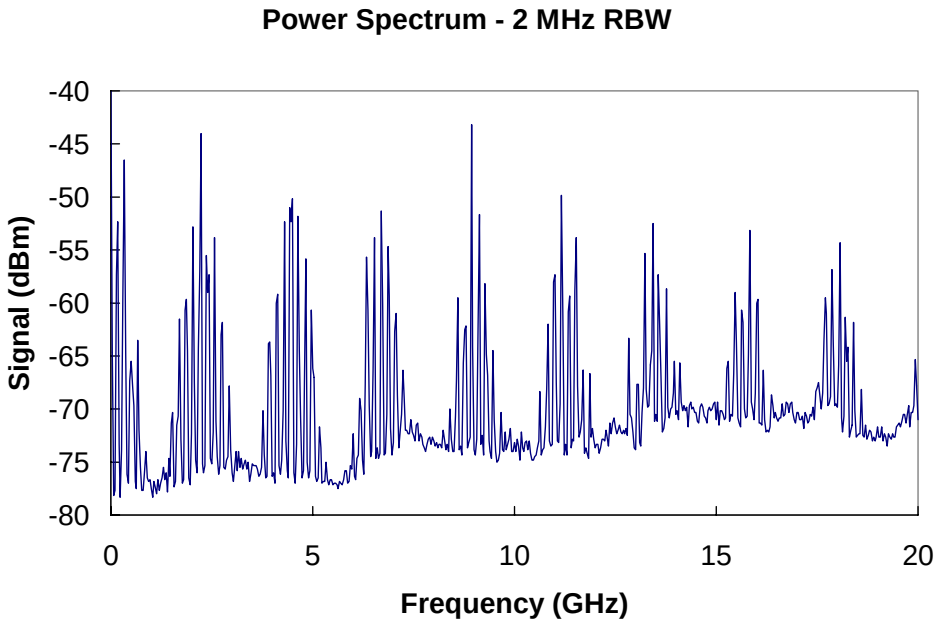

Figure 5. Power spectrum of the photodetected output of the laser array in the configuration corresponding to the optical spectrum in Figure 3. The resolution bandwidth (RBW) of the microwave spectrum analyzer (MSA) is 2 MHz.

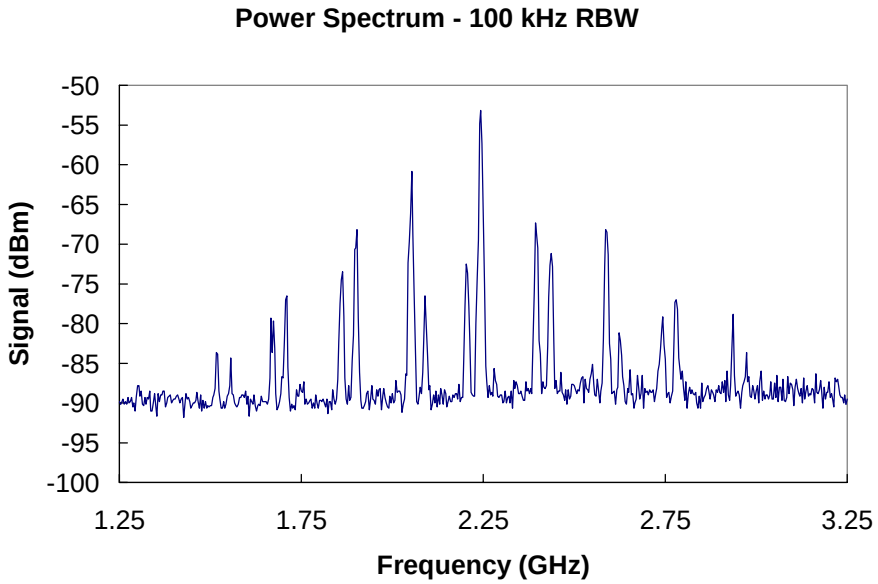

Figure 6. Detail of the power spectrum of the photodetected output of the laser array in the configuration corresponding to the optical spectrum in Figure 3. The RBW of the MSA is 0.1 MHz.

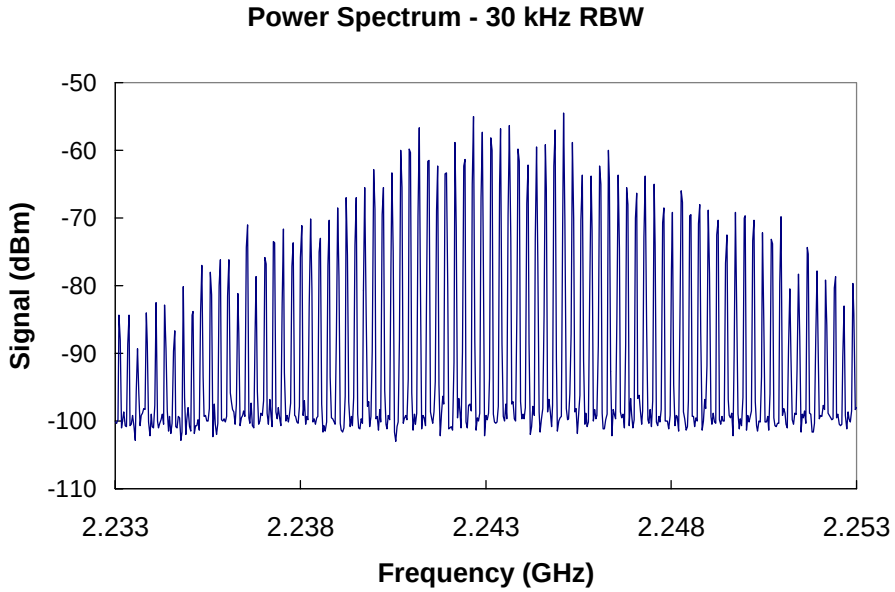

Figure 7. Detail of the power spectrum of the photodetected output of the laser array in the configuration corresponding to the optical spectrum in Figure 3. The RBW of the MSA is 30 kHz.

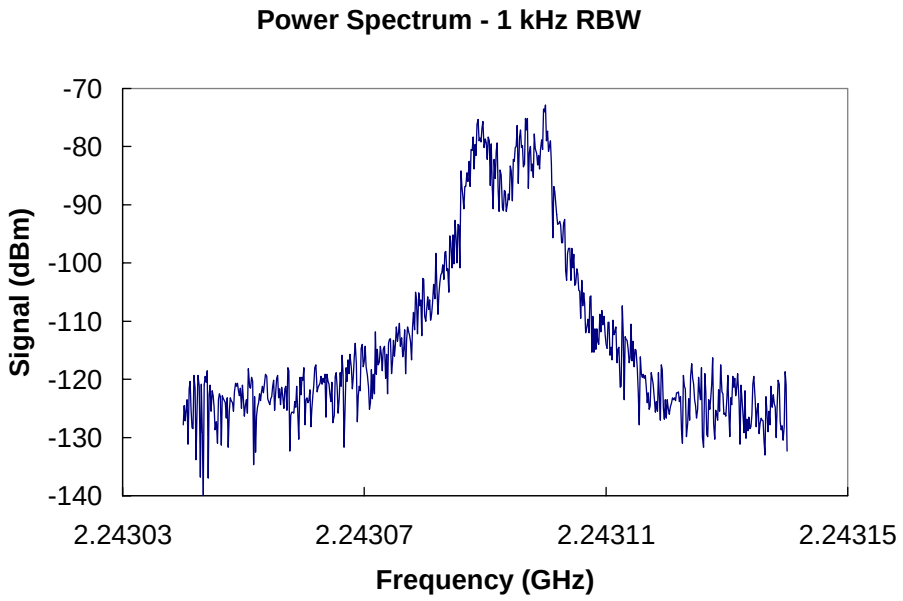

Figure 8. Detail of the power spectrum of the photodetected output of the laser array in the configuration corresponding to the optical spectrum in Figure 3. The RBW of the MSA is 1 kHz.

The structure is not evident for peaks at low frequency but becomes more pronounced as the frequency becomes larger. This indicates that the coupling between the cavity modes becomes weaker with greater frequency separation.

When a 30-m patchchord was added into one of the amplifier paths its associated ~7-MHz frequency spacing also became clear. We also observe that if the length mismatches became sufficiently close to being multiples, the shorter mismatch, higher frequency spacing would be evident but the other would be suppressed. However, only when the smallest cavity length mismatch became sufficiently short, ~1-cm mismatch, was there deviation from the pattern of spectral spacings associated with length differences. At this point, very few modes within the high reflection band of the FBG satisfy the laser round trip phase condition.

The high coherence of the combined laser output is shown by comparing the output power from the laser with the output from the "loss" port of the final 2 × 2 coupler of the tree of couplers and the output from the back end of the grating. Table 1 summarizes a typical result with the laser operating with the 90/10 output coupler configured to yield 90% feedback. All outputs are

normalized to the signals with a solitary amplifier operating. The actual power that leaked through the grating was considerably smaller than the output or loss port powers for one amplifier. The two-amplifier configuration was set up so that the beams were coupled in the same 2×2 coupler as the loss port measurement. The 8x increase in power from one to two amplifiers indicates that the losses form the extra fiber couplers make the one-amplifier configuration quite close to threshold at this pump level [6]. Coherent coupling reduces intracavity losses. Increasing from two to four amplifiers yields a 5x power increase that is closer to the 4x increase expected in the limit of pumping well above threshold. With all four amplifiers operating, greater than 95% of the circulating power is directed to the useful port of the 2×2 coupler for feedback and extracted power. It is important to remember that this is occurring even with the high frequency fluctuations in laser output due to the nonlinear mixing in the long cavities.

The good coherence is independent of whether there is a sparse or dense optical spectrum in the long cavity configuration. It is generally maintained even though the optical spectrum of the laser is varying over time with the changes in laboratory conditions. Over several hours of operation, the degree of coherence slowly drops but it can be restored by polarization adjustment. These results are potentially quite promising for the scaling of the system to large, high-power arrays. However, further work needs to be done to determine how the cavity length mismatches factor into the coherence in very large arrays. We have observed that the degree of coherence fluctuates strongly when the length mismatch in two-laser configurations drops to the centimeter range.

Table 1. Relative output power in four-laser configuration.

	Output	**Loss Port**	**Grating**
1 amplifier	1	1	1
2 amplifiers	8.2	0.6	0.5
3 amplifiers	21	2.4	1.2
4 amplifiers	43	0.9	1.4

4.0 NEW RESULTS WITH LINEAR 4- AND 5-AMP CONFIGURATIONS

With the ring-cavity configuration, we had seen no isolated spectral structure that we could associate with SBS. There was no 10.7 GHz structure in the spectra and the strong frequency components in the optical spectra were confined to the region of FBG high reflection. Of course, SBS is a counter-propagating signal and the unidirectional ring configuration prohibits build-up of such signals. Therefore, in the current program we switched to linear configurations, such as the one shown in Figure 9. The amplifier chains are combined through fiber-optic couplers. One end of all the amplifier chains is terminated with a high reflection FBG. Though we had five FBGs on hand, initially we restricted ourselves to the four with the best spectral overlap. Two of the 100 mW amplifiers are tied to the same FBG in a Mach-Zehnder configuration, because of a limited number of spectrally overlapping FBGs, while each of the other amplifiers had a separate FBG. Figure 10 compares the transmission minima of the four FBGs that were used. Care was taken to make all of the path lengths of the amplifier legs different by at least 10 cm, and care was also taken to make sure that the path length differences were not multiples of each other to less than 10 cm. This was done to be sure that the Fabry-Perot mode frequency spacing of each individual amplifier leg was different, and that overlap in frequency of multiple modes from the different legs was as non-periodic as possible. The amplifier chains are combined through trees of 2 x 2 fiber couplers. The output beam, now propagating in free space, is passed through a half-wave plate and a polarizing beamsplitter so that the polarization-resolved output can be measured. We also made measurements operating the 500 mW and combined 4x100 mW arms independently. When doing this, the 50/50 coupler to the common arm was removed so that it would not act as a loss port.

Figure 9 shows that the leg combining the 4 - 100 mW amplifiers is configured with a commercial 1 x 4 combiner/splitter. Before proceeding, we will comment on the polarization characteristics of the fiber couplers, in particular, and the long cavities, in general. We observed that for some of the amplifiers that the laser output in a single amplifier configuration had an elliptically polarized output. In general, the fiber polarization rotators, or simply twisting the fiber, could not induce the output to be transformed from linear to elliptical polarization. They appeared to simply rotate both polarization axes the same way. In this way the rotators can control the linear polarization axis. However, they cannot enforce linear polarization.

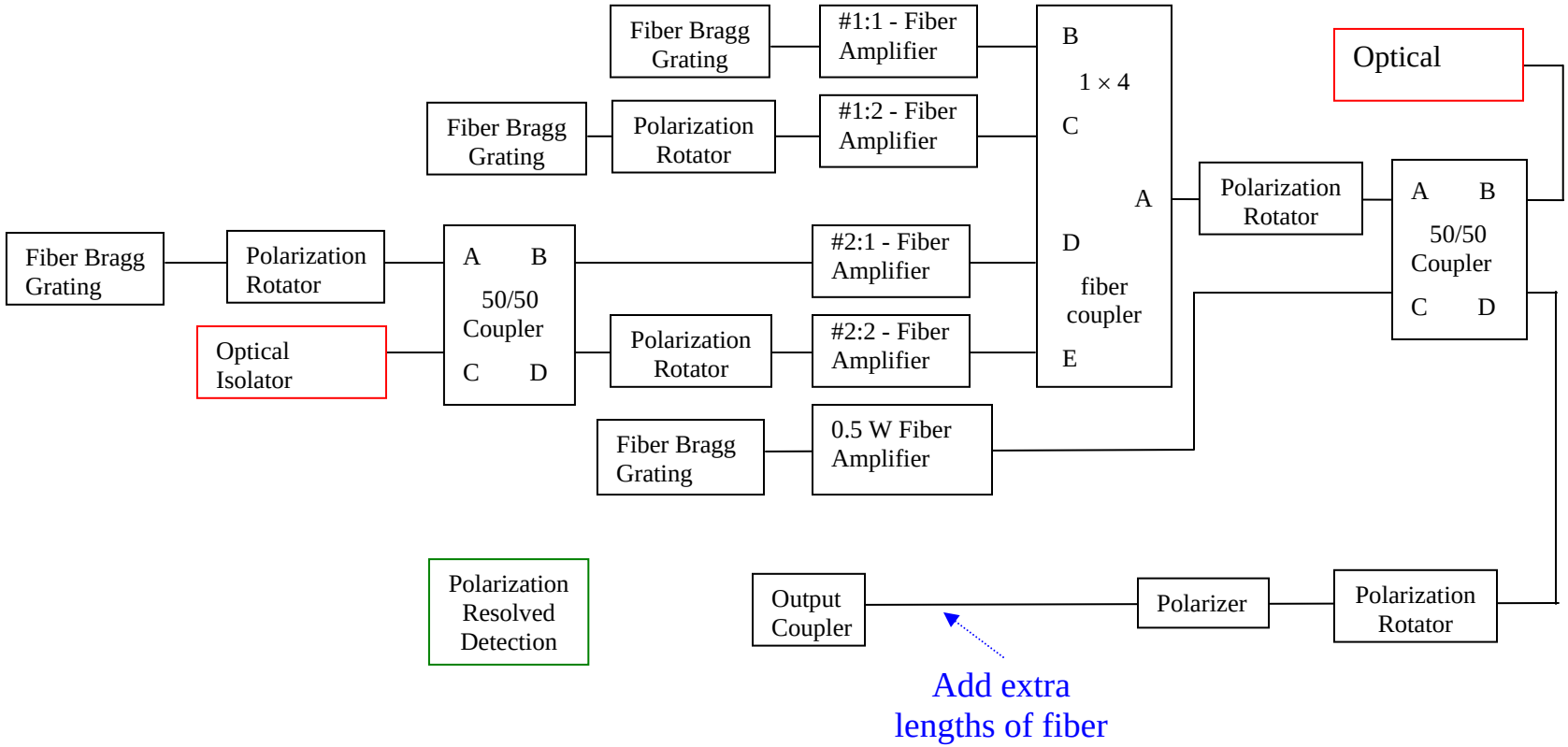

Figure 9. Schematic of the five-amplifier linear configuration.

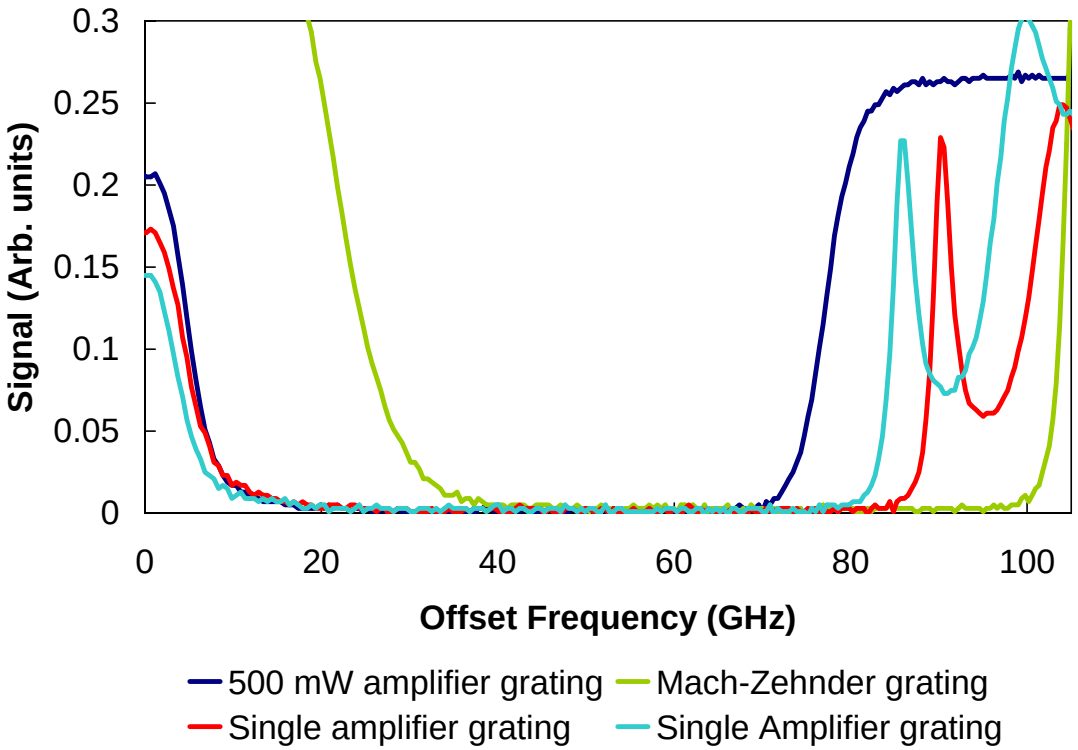

Figure 10. Transmission minima (approximate high reflection bands) of the four FBGs used to configure the array.

We next formed a two-element array, using two FBGs, two fiber amplifiers and a 50/50 fiber coupler, and observed that the 2×2 fiber couplers would sometimes cause two originally linear polarized inputs, based on single laser operation, to become elliptically polarized for maximum coherence. This is significant when one is trying to build a tree of couplers to try to induce coherence over many amplifiers. We observed that we were unable to achieve optimal coherence once the linear polarization was lost.

Proceeding on to a four-amplifier configuration, we used both a tree of 2×2 couplers or 1×4 couplers. When using commercially-available 1×4 fiber couplers, which consist of a tree of 2×2 couplers with some of the ends truncated as maximum loss points, we observed that linear polarization rotation on the amplifier arms and/or the common arm of the coupled laser cavity was insufficient to provide good coherent coupling. With a tree of three 2×2 couplers instead of the 1×4 fiber coupler the results were somewhat better, but still less than ideal.

Finally, we added the fiber polarizer to the common arm of a linear, four-amplifier configuration (four amplifiers and four FBGs). Once the polarizer enforced the polarization, we were again able to use the fiber polarization rotators to achieve good coherence in this configuration. The output was not steady, but the coupling efficiency was close to ideal, >90%. Therefore, to achieve good coherent coupling, linear polarization must be enforced, not just encouraged. Otherwise, the laser will parasitically couple power into the wrong polarization.

The results described above were made using a relatively short common path length, ≤ 5 m. As we hade observed with the linear cavity configuration, the mode and optical spectra of this short cavity, multi-element configuration were quite erratic. Once we achieved good coherence we then extended the common path length. Like the case of the unidirectional ring laser, the power spectrum broadened as we increased the path length. Further, we observed that the output power was only somewhat diminished, by less than 25% for the common cavity lengths up to 50 m, consistent with the additional losses due to the extra FC/APC couplers used with the additional fiber. As with the unidirectional ring cavity, stimulated Brillouin coupling between the forward and backward propagating waves did not play a significant role before phase coupling across laser modes produced the first clearly observable nonlinear effects. The backward traveling wave due to the ~1-3% reflection from the output coupling surface did not experience strong coupling to the forward propagating modes.

At any FC/APC coupling point there are losses due to imperfect matching of the mating fibers. Typically, these can range up to 0.5 dB. Because the coupling of two lasers typically involves the addition of at least two FC/APC coupling points, we observe that a maximum coherently coupled output powers are only 80-90% the expected level due to the losses at the fiber couplers. This is true even when the "lost" power at the 2×2 coupling arm is quite small. This is the price that we pay for the flexibility of the experimental apparatus. Over time we concluded that this price was too high and has severely limited our progress. This makes some quantitative comparisons with the larger arrays difficult because we are using 1×4 couplers where we cannot monitor the loss arms. Ideally, one should use only full trees of 2×2 couplers to be able to monitor all loss points. We further observed that coupling points become lossy over time at the power levels (hundreds of milliwatts) that we use. Often this is due to coupling and uncoupling the fibers. Even though problem is not apparent when the fiber coupler end is inspected, we have observed damage soon

after. We believe that the many spurious etalon effects that we observed in the past are due to the losses and scattering that can occur at imperfect FC/APC coupling points. The only nonlinear effects that we have unambiguously observed within the high reflection bandwidth of the FBGs are the spectral broadening effects due to the cross phase modulation of the laser modes in the long fiber cavities. Later, we will describe observation of SBS output outside of this spectral region.

Now, back to the five-laser configuration made by combining one 500 mW laser arm with 4 x 100 mW coupled lasers. This configuration combined Michaelson and Mach-Zehnder type coupling in the linear configuration, using four FBGs for the five amplifier arms. Good coherence was achieved, though the coherent power never exceeded 500 mW due, we believe, to the extra losses in all the contact points of the array configuration. This linear configuration displayed the same kind of spectral behavior that we observed in the ring configuration. Figure 11 shows the optical spectrum generated by the five-element array, as well as the spectrum of the two main sub-components. Note that the spectrum of the combined array is shifted relative to both the principal components. The structure due to length mismatches is

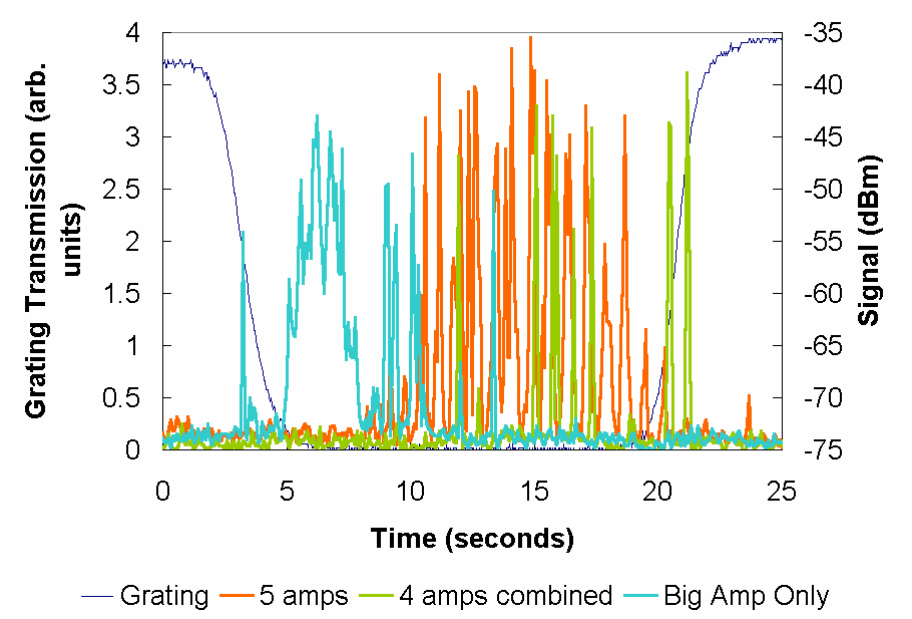

Figure 11. Optical spectra of the laser output taken by scanning a heterodyne laser optical frequency across the output frequencies. The gating has a stop-band for transmission of ~ 45 GHz, so that the scan covers ~ 3 GHz/s. The grating shown for comparison is the one used in the 500 mW amp arm.

clearly evident in the multi-element spectra. Also, by paying attention to the coupling points, we could confirm that the etaloning was due to parasitic reflection points in the fiber. Therefore, the spectral broadening is the only nonlinear optics effect that we have observed in arrays with a high-reflection spectral band with a width > 30 GHz.

We observed that the mode coupling in very long cavities includes coupling of orthogonally polarized modes. With long cavities, we achieved the best coherent coupling when the polarizer was placed near the end of the long common arm. However, the laser output was typically elliptically polarized during the long round trip so that the good coherence was mitigated by the fact that we could not achieve as high output power levels in the longer cavities. Using one 500 mW amplifier and coupled with a cascade of 4 – 100 mW amplifiers, we have been able to achieve linearly polarized output power levels approaching 500 mW in cavities up to ~ 70 m in length. The maximum power dropped below 300 mW when the cavity was increased to 400 m. The power spectrum of the 400 m laser showed a spectrum consisting of two offset sets of modes, consistent with polarization mode dispersion in the fiber, and evidence of the polarization scrambling induced in the long fiber. Broadened, but not polarization scrambled, spectra were observed at these power levels with the 70 m laser array. Therefore, there appears to be an optimum degree of nonlinear coupling before the deleterious polarization scrambling effects set in.

We next varied the path length between the polarizer and the output coupler by adding extra lengths of fiber. We made measurements on cavities with ~ 20, 70 and 420 +/- 10 m of fiber total length. Approximately 2% of the beam is reflected at the facet back into the single-mode fiber. Figure 12 compares the optical spectra of the coherently combined output from the five-amplifier configuration for different cavity lengths, where the extra fiber is added to the common arm. The grating transmission for the 500 mW amplifier grating is also shown for reference. All show considerable structure, but the spectral features generally broaden as the cavity length increases. This is particularly apparent in the longest cavity spectrum. Note that the spectra remain approximately centered in the region where all gratings have high reflectivity. If we compare this with the situation when either the 500 mW amplifier or the combined 4x100 mW amplifiers are run separately, we observe that there is a pronounced shift in the spectra, as shown in Figure 13. The four-amplifier spectrum is shifted to higher frequencies, and the 500 mW amplifier spectrum

to lower frequencies, due, most likely to the relative shifts of their respective FBGs. This is one of many indicators of the coherent operation of the multielement array.

Further evidence of the coherence and the spectral broadening in longer cavities is given by the output power spectra. Spectra for the three different cavity lengths are given in Figure 14. They are taken by setting the microwave spectrum analyzer on the peak hold setting and taking many sweeps. This effectively produces an average. There is considerable broadening of the peaks at both the 70 m and 420 m cavity lengths. More detailed spectra showed that individual peaks are separated by the cavity mode frequency and that the general spectral structure appeared to be consistent with the different cavity length mismatches of the different amplifier paths.

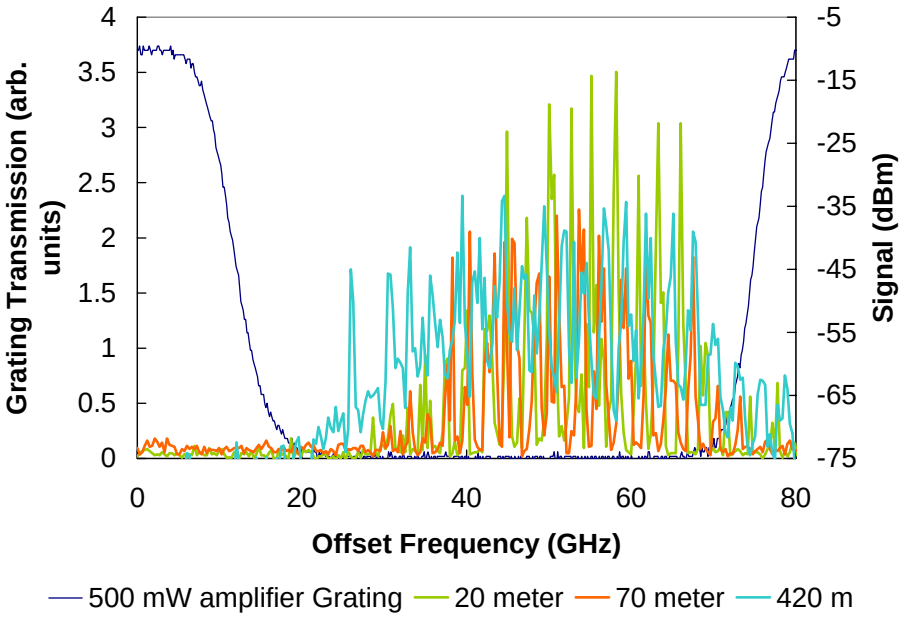

Figure 12. Output optical spectra of the 5-amplifier array for different cavity lengths, compared to the transmission stop band of the 500 mW amplifier FBG. The signal power is in a logarithmic scale (right axis). The frequency axis is relative to an arbitrary offset.

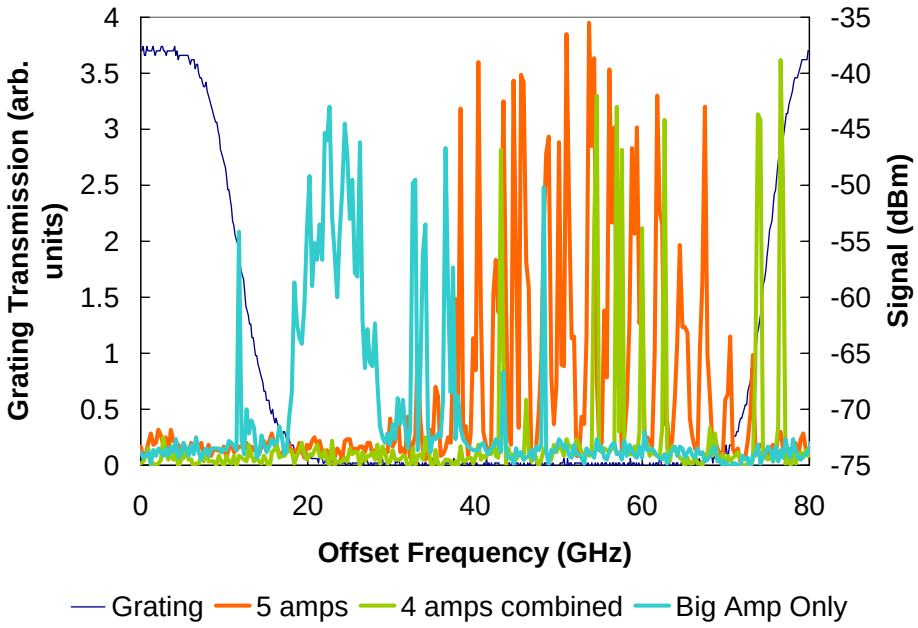

Figure 13. Optical spectra of the laser output taken by scanning a heterodyne laser optical frequency across the output frequencies, compared to the transmission stop band of the 500 mW amplifier FBG. The signal power is in a logarithmic scale (right axis). The frequency axis is relative to an arbitrary offset.

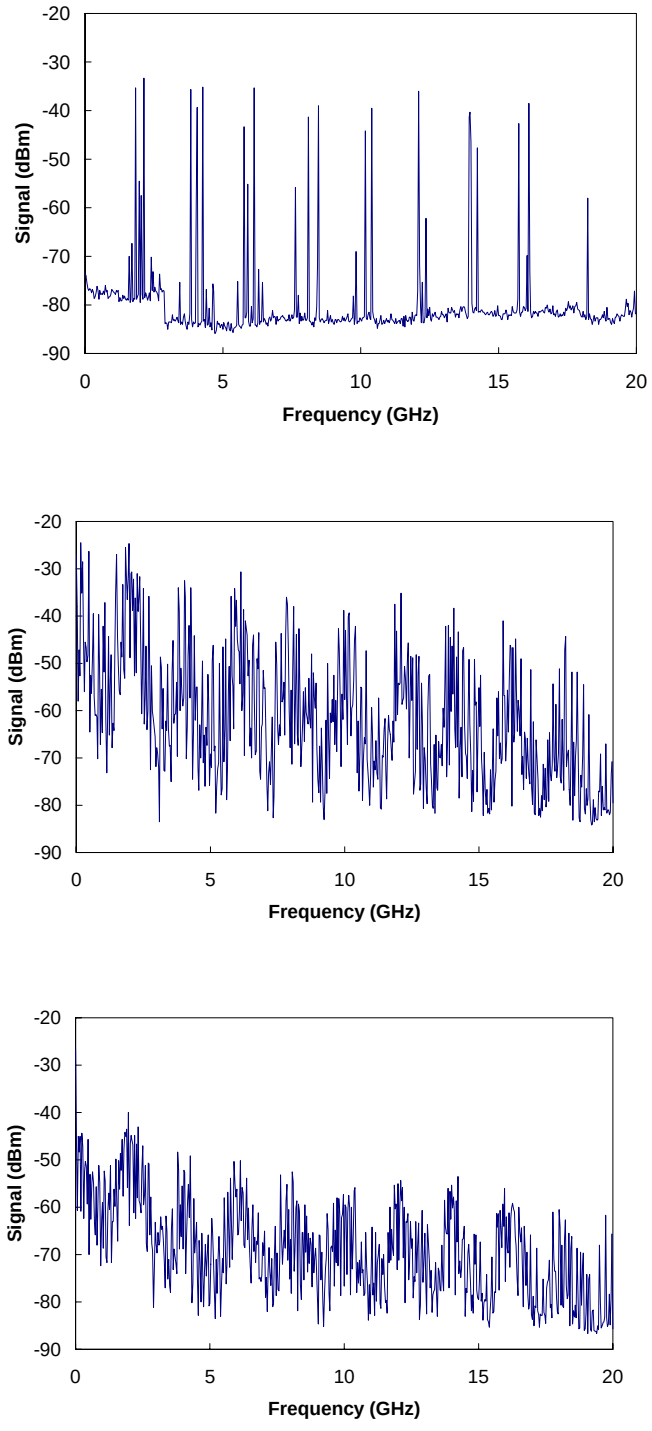

Figure 14. Power spectra of the 20 m (top), 70 m (middle) and 420 m (bottom) arrays. The spectrum analyzer used in the measurement was out of calibration and this caused a step in the signal power at ~ 2.9 GHz that is most visible in the top spectrum.

5.0 INVESTIGATIONS OF INTRACAVITY ETALONS

While we were able to observe the coherent combining, the spectra tended to be erratic and complicated by the etaloning effects. Therefore, we decided to systematically study etaloning by creating etalons in a simple configuration. We returned to the unidirectional ring laser configuration that we have previously developed, and set up a single-amplifier cavity with an extra coupled passive fiber loop as shown in Figure 15. Both the length of the loop and the losses in the loop could be varied. The main fiber loop was made quite long, over 400 m, so that the density of lasing modes would be high. We set up this passive loop to investigate the effects of parasitic reflectivities within the laser cavity. We had observed etalon-like effects in spectra previously generated. However, there should have been no reflection points with $R>10^{-3}$ in the cavity. Due to the passive loop, the power spectra of the photodetected output displayed repeating structure at multiples of frequencies corresponding to c/l where c is the speed of light and l is the loop length. As expected, the depth of the fringes decreased with increasing attenuation and once the loop attenuation exceeded 10^{-4}, there were no significant etalon effects. The length of the passive loop did not change this. Therefore, it seems most unlikely that parasitic etaloning between reflection points with $R<10^{-3}$ (two would be required to form the etalon) could account for spectral structure.

We did observe unexpected phenomena related to polarization in the fiber loop. We initially inserted a polarization rotator in the loop as a mechanism for fine control of the attenuation. With the polarizer in the main cavity loop, changes in polarization should lead to effective changes in strength. The attenuation effects were observed but so were additional spectral effects. Figure 16 shows some different power spectra that were observed. Etalon structure at sub-harmonics of the basic loop length frequency is clearly observed. It appears that with the proper rotation of polarization in the fiber loop, multiple round trips could yield efficient coupling to modify the laser spectra. Again however, the signals in the loop had to be > -30dBc to influence the spectra. As the loop length was increased by a factor of 2-3 the higher order sub-harmonics were harder to generate, with only the period doubling visible for a loop length of ~ 12 m, and only the fundamental period for a loop length of 34 m, both still very short compared to the main cavity loop.

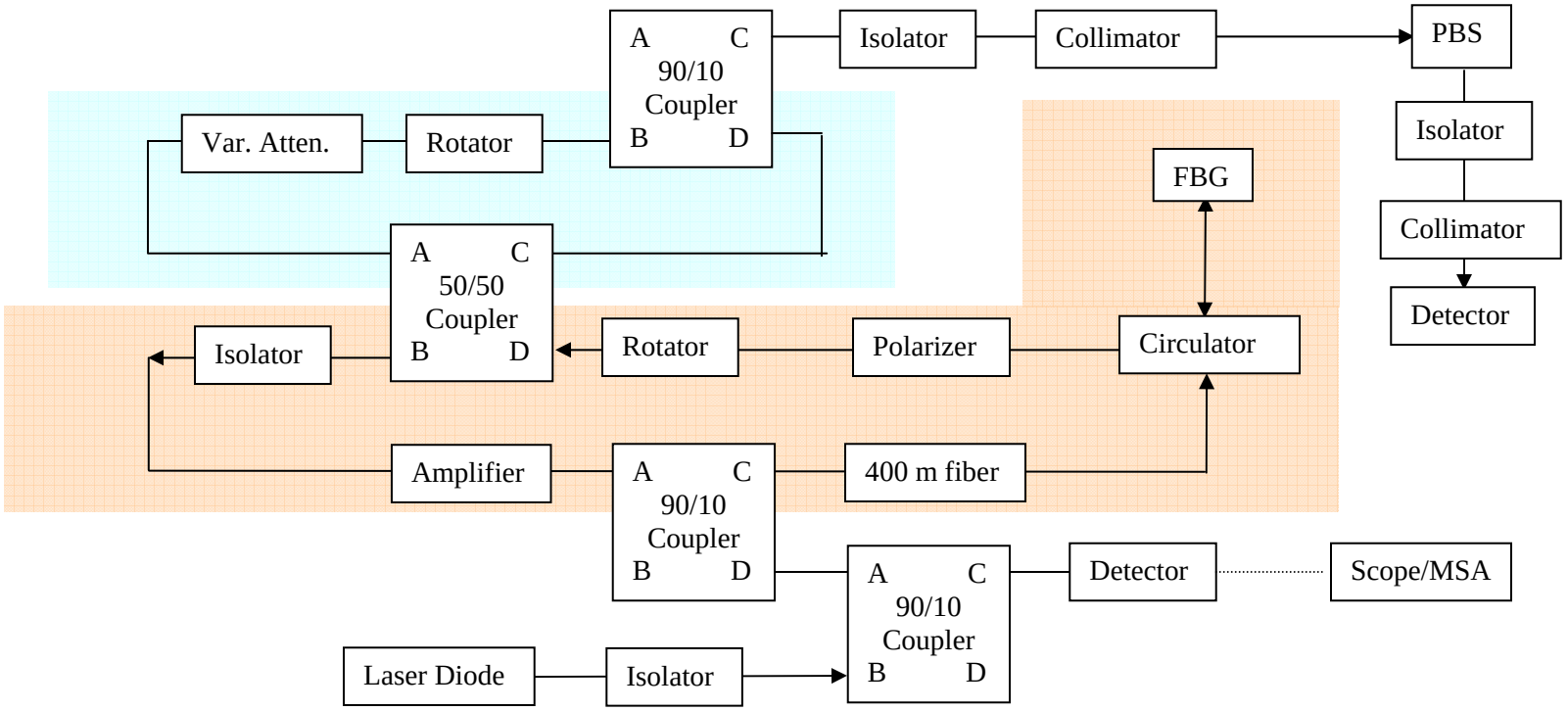

Figure 15. Schematic of the experimental apparatus used to investigate parasitic etalon effects in a ring cavity. The main laser cavity, a unidirectional ring cavity, is highlighted in tan. A separate ring that acts to mimic a parasitic etalon in the cavity is highlighted in blue. Both the main laser cavity and the ring can be monitored. In the configuration shown, polarization resolved detection is used to monitor the ring and an oscilloscope or microwave spectrum analyzer monitors the main cavity. Optical spectra of the main cavity output can be recorded by mixing with a laser diode that is scanned across the Bragg Grating high reflection spectral region using temperature control. This is easily interchanged by swapping fibers at the appropriate couplers. FBG = Fiber Bragg Grating, PBS = Polarizing Beam Splitter.

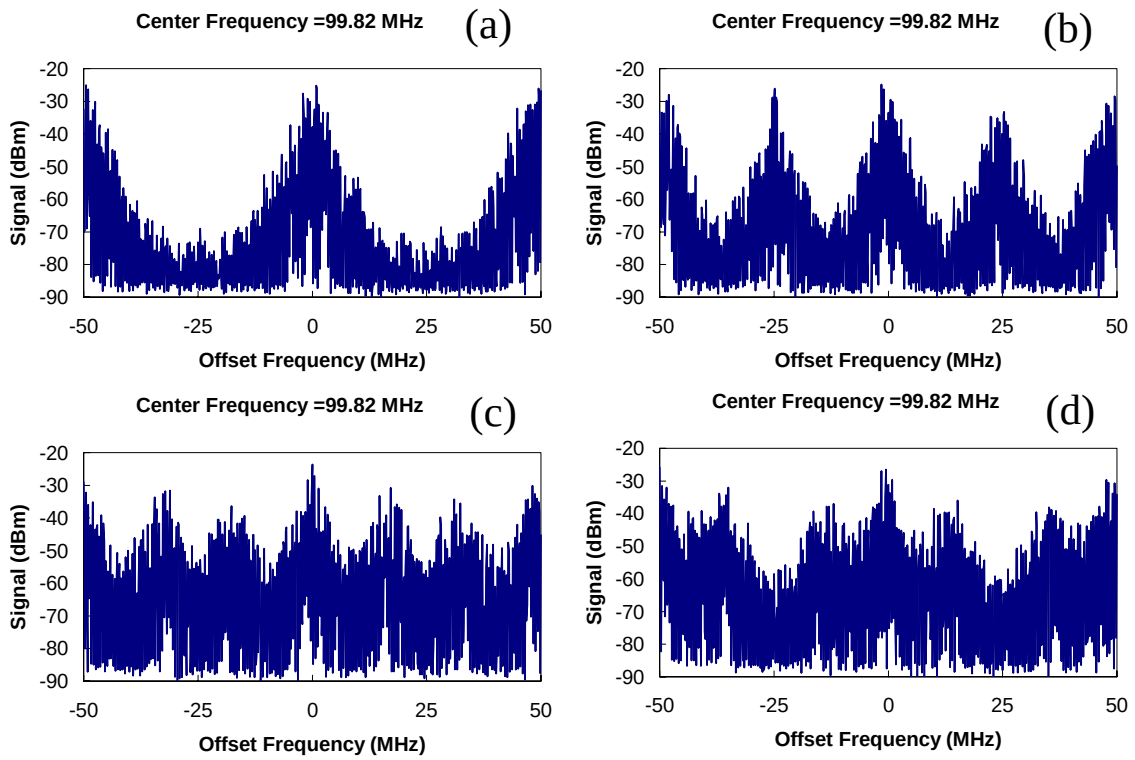

Figure 16. Changes to the power spectra when the polarization is rotated in the passive fiber loop. Figure (a) shows the basic loop mode frequency of 50 MHz, corresponding to a ~ 4 m loop. (b)-(d) show spectra with sub-harmonics that were generated by rotating the polarization of the signal in the loop.

To try and better understand what was causing these etalon effects, we constructed a time domain reflectometer to try and pinpoint the source of the intracavity reflections. A schematic to illustrate the set-up is shown in Figure 17. A distributed feedback laser diode is used as the probe source. It is optically isolated and pulsed to deliver a short, ~ 10 ns, light pulse into the fiber. Part of the light is detected by a trigger detector that is used to trigger a fast oscilloscope that monitors all photodiodes. The rest of the light is passed into the laser apparatus of fiber components under test. The return signal from that output is monitored by a fast photodiode. In Figure 17, the components of a laser cavity are shown under test. The DFB laser is tuned near but not within the high reflection stop band of the FBG that forms the cavity end reflector. By operating near the stop-band a small portion of the laser signal is reflected by the FBG. This gives a marker for the beginning of signals from the laser cavity. Weak reflections from any of the FC/APC connection points within the laser cavity beyond the amplifier medium receive a double-pass amplification by the fiber amplifier. Typically, we adjust the amplifier gain to be

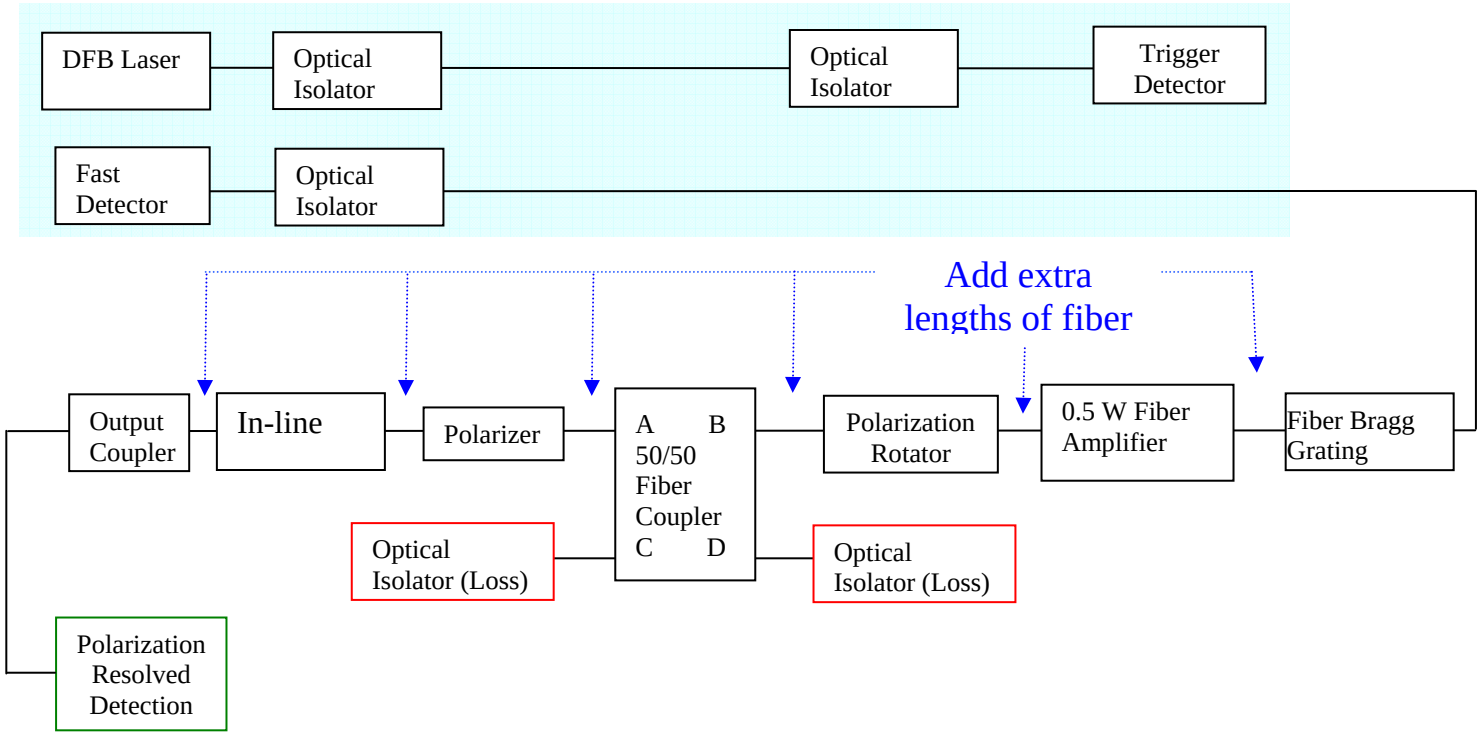

Figure 17. Schematic of the fiber reflectometer and laser configuration. A distributed feedback laser diode is tuned to operate near but not within the high reflection stop band of the FBG. The laser is pulsed with a short (~ 10 ns) pulse. The pulse is detected by a trigger amplifier. Weak reflections from the FBG and from the attenuated reflection signal from the output coupler define the time window of possible reflections from within the laser cavity. Extra lengths of fiber are added to isolate individual coupling points.

just below threshold so that the is significant round trip gain but not enough to support oscillation. At the far end of the laser cavity, the output coupler provides a reflection signal of known strength. Approximately 2% of the light incident on the output coupler from the fiber is reflected back into the cavity. This signal is sufficiently strong that it must be attenuated. We are able to distinguish point reflections down to below –50 dB. Therefore, a good FC/APC connector does not provide a resolvable signal. However, we would typically observe weak signals from points within the cavity, Often they could be eliminated by careful cleaning and polishing of the connectors. However, some connections always showed a residual reflection and we were able to correlate etalon spectral features with these parasitic reflection points. At variance with our earlier results where we explicitly configured an intracavity etalon, we observed that parasitic reflections below –40 dB led to significant measurable etalon effects in intracavity coupled lasers. Our previous etalon tests were done with an etalon in a single amplifier configuration and there was no amplifier in the eparate etalon arm in those tests. Perhaps, that test was not sensitive enough to show the effects in the coupled cavity configurations.

The reflected signal sometimes changed after we disconnected and reconnected an FC/APC connector. It could also vary over time, possibly due to heating effects at the connector. As we have moved from 100 mW fiber amplifiers to 500 mW fiber amplifiers during the course of this investigation, we have spent more time tracking down the intracavity parasitic etalons. Apparently, the same power levels that lead to the appearance of the fiber nonlinearities in the long cavities also are more likely to cause some damage in the optical surfaces at the FC/APC couplers.

Therefore, there appears to be a relatively stiff price to pay for the ability to quickly reconfigure the laser configuration. In the future, it would be worthwhile to invest in a fusion splicer to eliminate some of the intracavity connectors. However, by the time the data clearly showed this, the capital equipment purchase of the fusion splicer was beyond the resources available, so we continued to work with the apparatus on hand and to choose among our components to minimize the etaloning.

6.0 OBSERVATION OF SBS

The output from four-and five-element linear array cavities was similar to the output from ring cavities and that there was no obvious spectral signature for SBS. This was puzzling given the relatively low SBS threshold power relative to the intrinsic Kerr nonlinearity of the optical fiber, but can be explained by noting that the laser power is spread over many optical modes in the long cavities that we were using. Therefore, we next worked to confine the laser output to a narrower spectral range with the hope of observing the SBS peak.

We concentrated on one- and two-amplifier configurations using the high-power, 500 mW Erbium-doped fiber amplifiers. The spectral range of the laser cavities was controlled through the use of FBGs. Figure 18 shows the relative frequency ranges of the five FBGs that we have acquired. All are centered between 1557.2 and 1557.4 nm. To date, we have used up to four

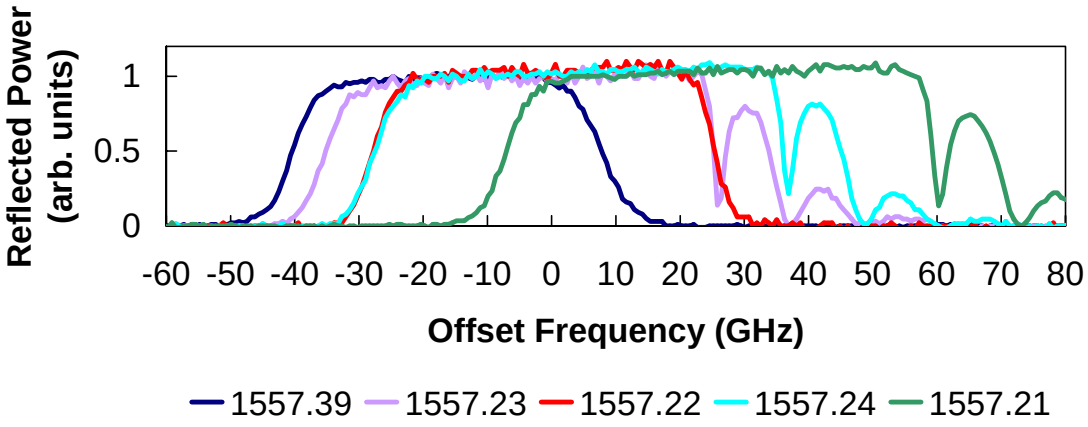

Figure 18. High Reflectance spectra of the FBGs.

gratings simultaneously and avoided using the 1557.21 and 1557.39 gratings at the same time due to their relatively narrow spectral overlap. Very early in this investigation, we achieved poor coherence in multilaser configurations that combined these two FBGs. However, by restricting this part of the investigation to one- and two-amplifier configuration, we expected, at indeed observed, good results. When the grating labeled 1557.39 is combined with the one labeled 1557.21 there is only a relatively small range of spectral overlap. Coherent output centered on the grating overlap would induce SBS only outside of the range of simultaneous high reflection for the two gratings due to the expected 10.7 GHz frequency shift of the SBS. Schematics of the laser configurations are shown in Figure 19. The one-amplifier configuration used two FBGs,

one at each end of the cavity. The two-amplifier configuration was in our standard linear-cavity coherent coupling configuration with a separate FBG end mirror for each amplifier. Various photodiodes were used to monitor the output through the intended output coupler, the loss ports and the leakage through the FBGs. Short lengths of fiber were inserted into the two amplifier arms of the two-amplifier array to control the relative path length difference of the two coupled cavities. The overall path length was over 400 m, and corresponded to a mode spacing of ~ 250 kHz.

Optical spectra from the one-laser configuration are shown in Figure 20. The cavity end mirrors were formed by the FBGs labeled 1557.39 and 1557.21 in Figure 18. The main peak is confined within the region where both gratings display high reflectance. There are many optical modes oscillating simultaneously, and the mode amplitudes display large fluctuations with time. Offset from the main peak is a weaker, narrower peak and the offset is consistent with that expected for SBS. By observing the leakage light transmitted through the 1557.39 grating, where the main peak and SBS peak are preferentially blocked, we also generated spectra showing a weaker peak oppositely offset that corresponds to the anti-Stokes SBS peak. This is clear evidence of SBS in our long cavity configurations.

Optical spectra from the two-amplifier configuration are shown in Figure 21. Here, spectra from three different grating pairs of the coherently coupled lasers are shown. In all cases, the main peak is confined to the region of spectral overlap. However, the pair with the narrowest overlap clearly displays the offset SBS peak. The other two show enhanced features at the long wavelength side of the overlap region that may correspond to SBS but the picture is more ambiguous. Figure 22 shows the power spectrum for the narrowest overlap pair and one of the broader overlap pairs. In the former, peaks at multiples of ~ 900 MHz, corresponding to a path-length difference for the two amplifiers of ~ 11 cm, are observed. Matching the optical spectra, there is a second, weak set of peaks around 11 GHz, corresponding to the SBS offset. The spectra from the pair with the broader spectral overlap shows a somewhat different length mismatch and any SBS features are obscured by the broad spectral content of the main feature. Note that the peaks of the SBS offset feature are also harmonics of the 900 MHz cavity length mismatch frequency, with 10.7 GHz being close to one of the harmonics.

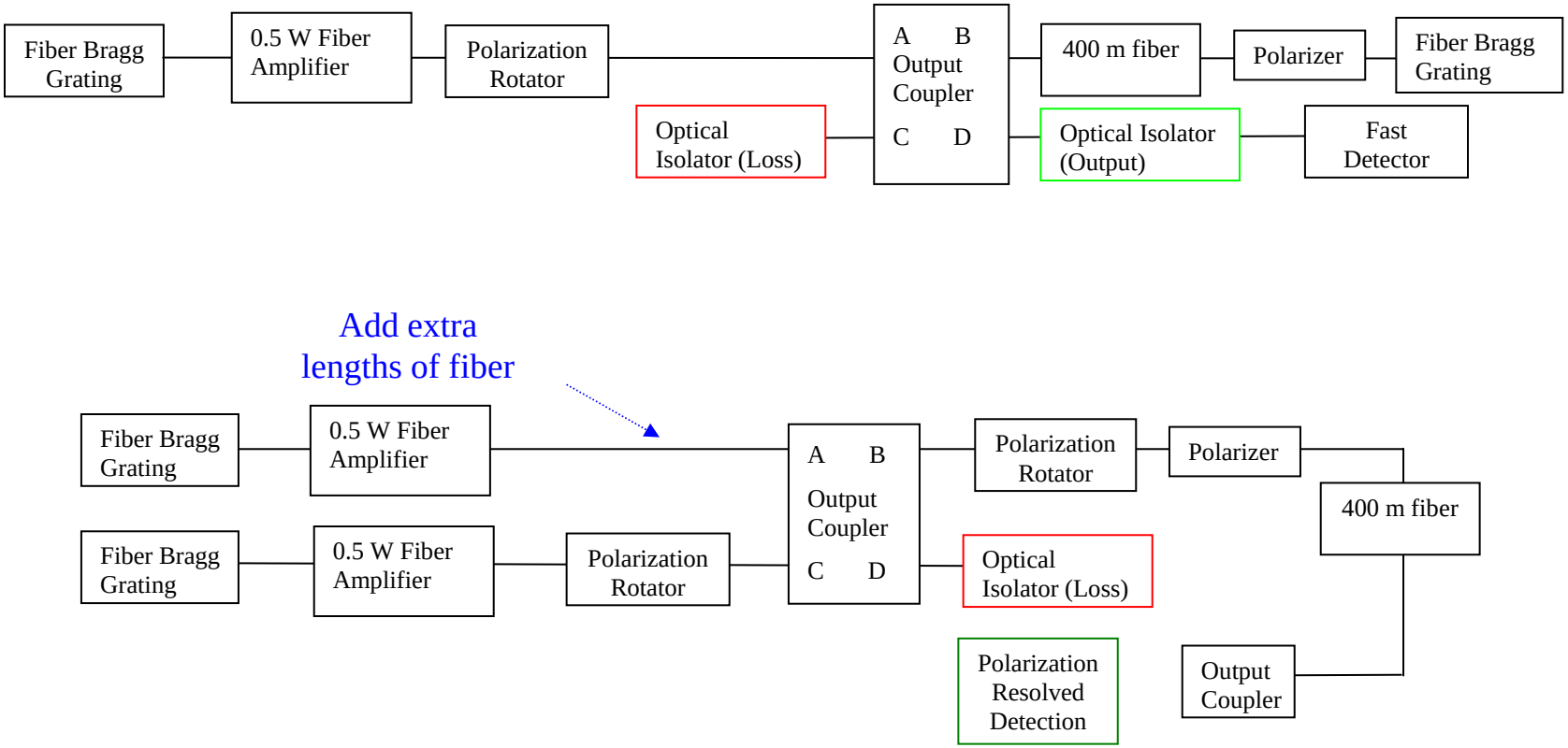

Figure 19. Schematic of the laser configuration. Top, one-amplifier configuration with wavelength selective gratings at each end of the cavity. Bottom, two-amplifier configuration with intracavity coherent coupling. Extra lengths of fiber were added to vary the path length difference in the two-amplifier configuration.

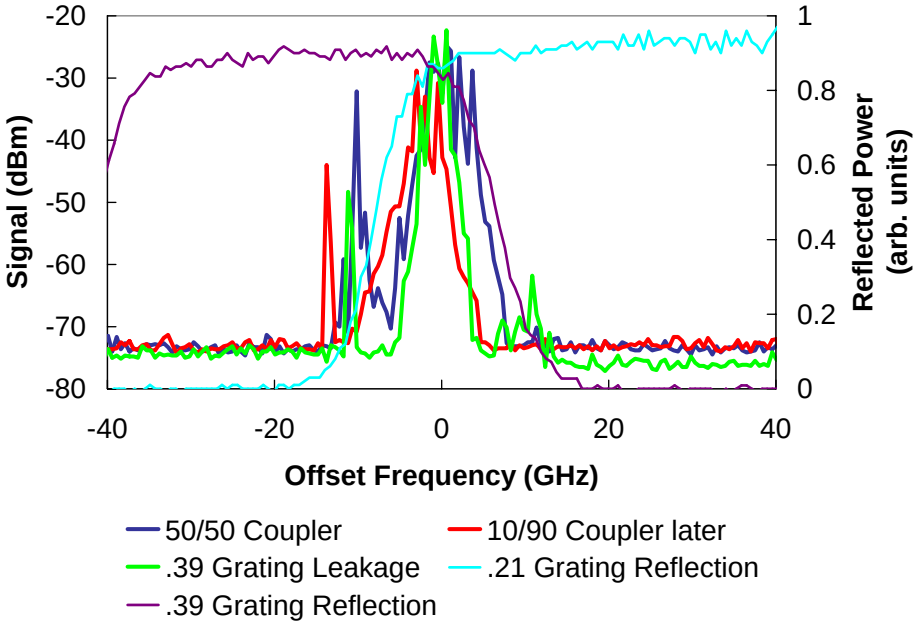

Figure 20. Optical spectra showing the output of the one-laser configuration. The spectra show a dominant optical feature at the overlap of the high reflectance regions of the two FBGs. Similar spectra were observed for two different output couplers (red and dark blue curves). The leakage through the longer wavelength grating (green curve) showed a weak anti-Stokes SBS peak in addition to the Stokes SBS peak observed in the output coupler spectra. Reflectance spectra from the two gratings are also shown for reference.

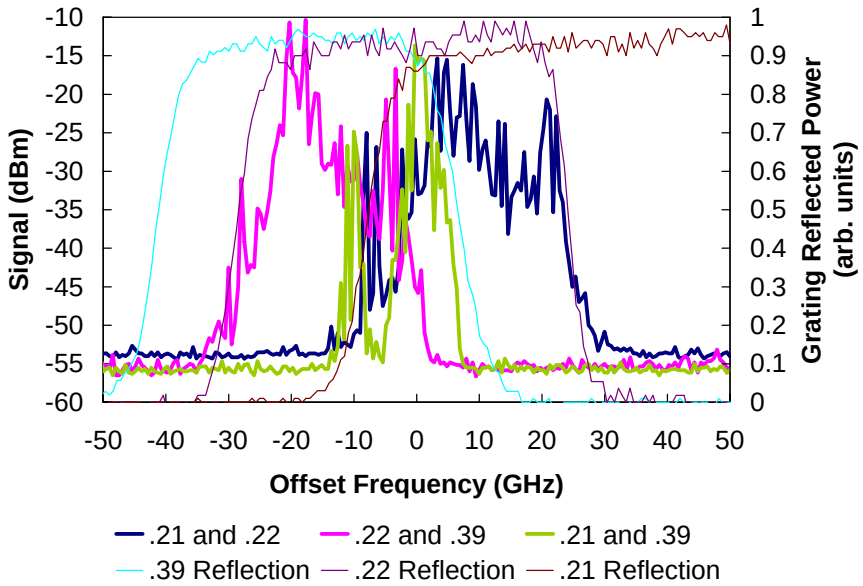

Figure 21. Optical spectra of two-amplifier coherent configuration. The dominant optical output is confined to the region of spectral overlap of the two gratings. The configuration with the narrowest overlap clearly shows an offset SBS peak.

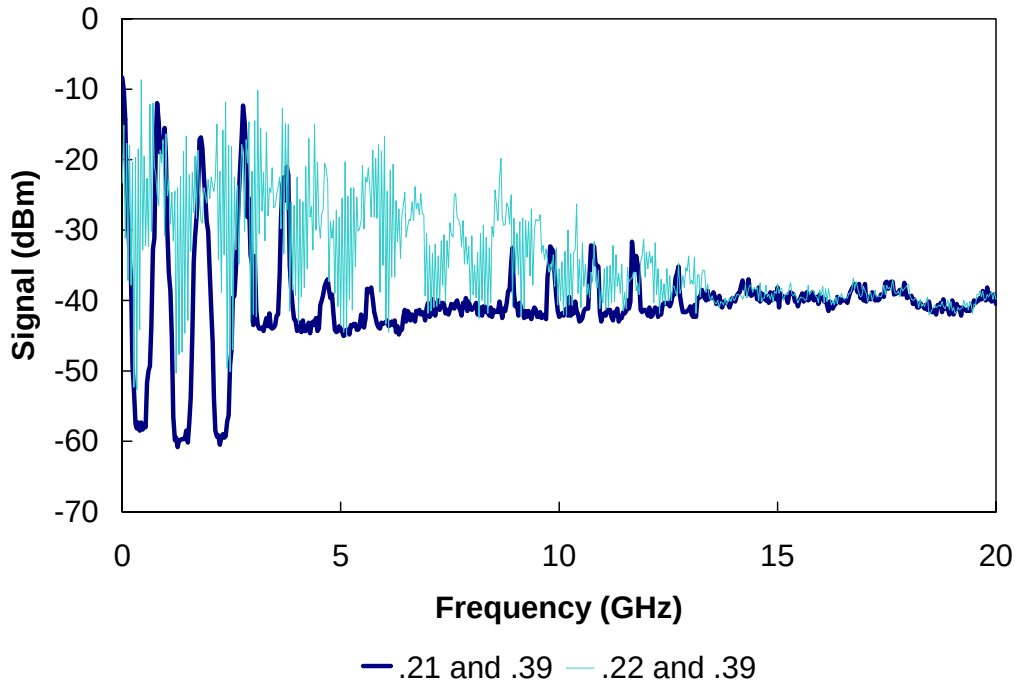

Figure 22. Power spectra corresponding to the optical spectra in Figure 21 labeled with the same FBGs in the two-amplifier configuration. Both display structure due to the length mismatch, though the configuration with the narrow spectral overlap is much cleaner. This configuration also clearly shows the SBS offset features near 11 GHz that are multiples of the length mismatch frequency.

Concentrating now on the two gratings with the narrowest spectral overlap, we varied the power circulating in the coupled configuration by adjusting the pump level of the two amplifiers. Optical spectra are shown in Figure 23.While both the broadening of the main spectral feature and the strength of the SBS feature decreased with decreasing power, the SBS feature disappeared at power levels where some broadening was still observed in the main feature. This further supports our previous data that the mode-to-mode cross phase modulation of the fiber Kerr nonlinearity is the first and dominant nonlinearity in the long fiber cavities.

We also varied the length mismatch between the amplifiers of the coupled array. Figure 24 shows two optical spectra at a length mismatch of ~ 3 cm. Here the output switched irregularly from a spectrum with a single dominant spectral feature in the region of high reflectance overlap to one where two or three features could be observed. The switching occurred on time scales of the order of a second and appeared to correlate with environmental changes in the lab, faster changes occurred when the room temperature was changing more quickly. The power spectrum

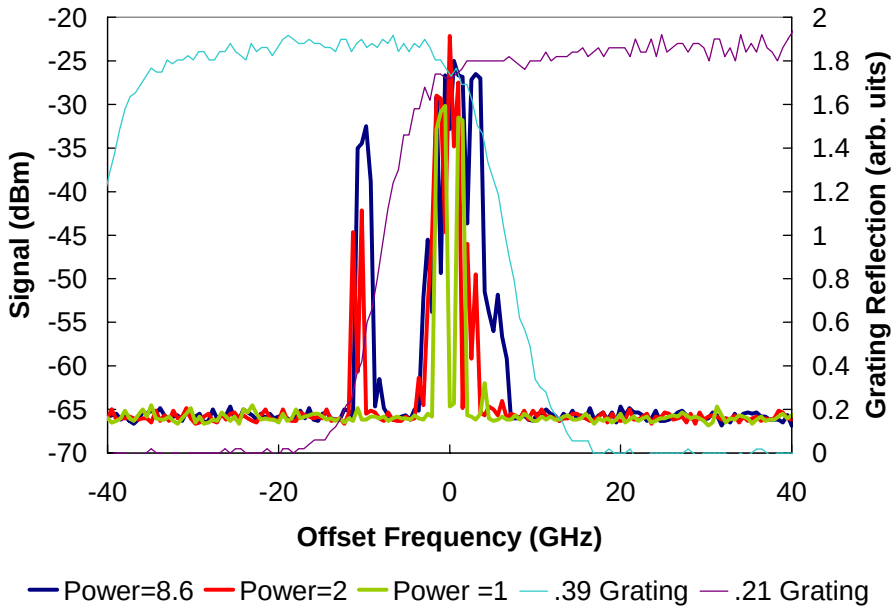

Figure 23. Changes to the optical spectra of the two-amplifier configuration using the gratings with the narrowest spectral overlap. The SBS peak is too small to be detected at the lowest power level where there is some broadening of the main spectral feature.

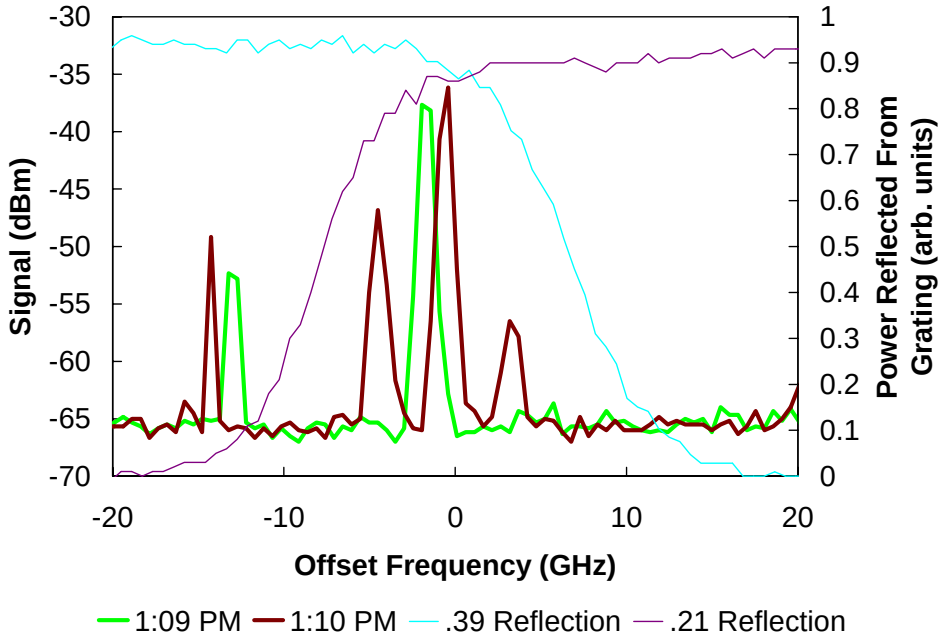

Figure 24. Optical spectra of the two-laser configuration where the length mismatch between the two amplifier paths has been reduced. The output now randomly varies between single and multiple features in the high simultaneous high-reflection region, with the offset SBS peak.

associated with the multipeak output is shown in Figure 25. The spectrum was taken using the max hold feature of the spectrum analyzer and repetitively triggering the trace. Single shot spectra with only the low frequency feature were observed. These, we believe correspond with the single peak optical spectra.

We could achieve fairly reproducible spectra for path length differences down to about 2 cm, corresponding to beat frequencies of ~ 5 GHz. When the beat frequency increased to 7 GHz, the spectra became much more erratic. 5 GHz is approximately half the frequency offset of the SBS peak, and this may be significant though further work is necessary to establish this.

Further spectra are shown in Figures 26 and 27. In the optical spectrum, we see a strong spectral feature approximately centered in the region where the high reflection bands of the two FBGs overlap, and a weaker feature offset a lower optical frequencies. From the power spectrum, Figure 27, we can determine that the length mismatch between the two lasers arms was ~ 10.5 cm. This yields the ~ 0.93 GHz spacing between strong peaks. The four peaks in the power

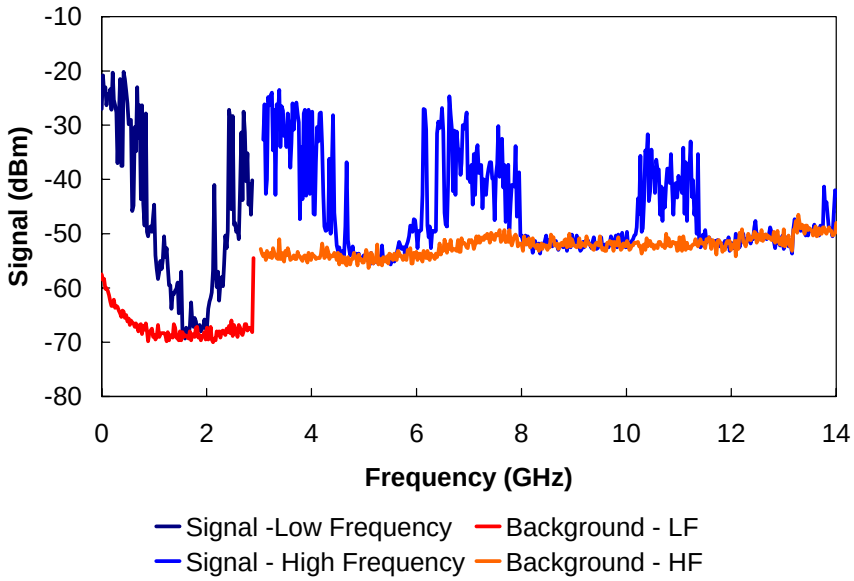

Figure 25. Power spectrum in the same configuration as the optical spectra of Figure 24. This trace is made running the spectrum analyzer in the peak hold setting. There is a calibration problem with the spectrum analyzer that causes the increased noise at higher frequencies.

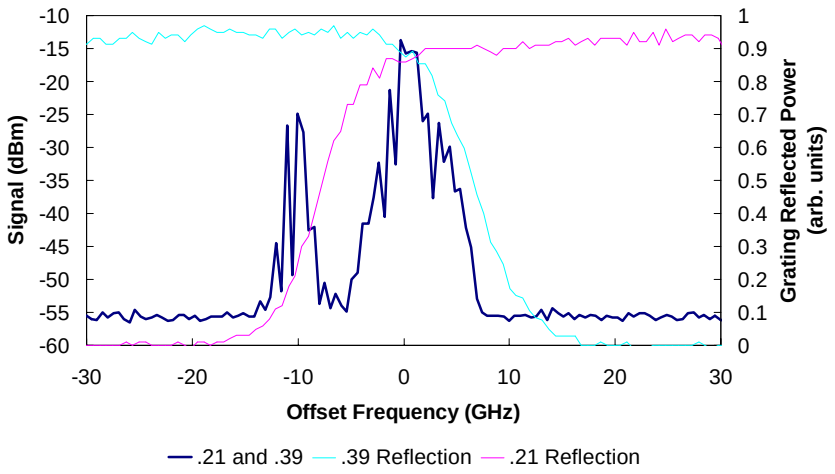

Figure 26. Optical spectrum of the coherently coupled array output. Also shown are the relative refectivities of the two FBGs used as high reflectors in the two arms. Note that the main spectral feature is the region of simultaneous high reflectivity while the offset feature is only in the high reflection region of one.

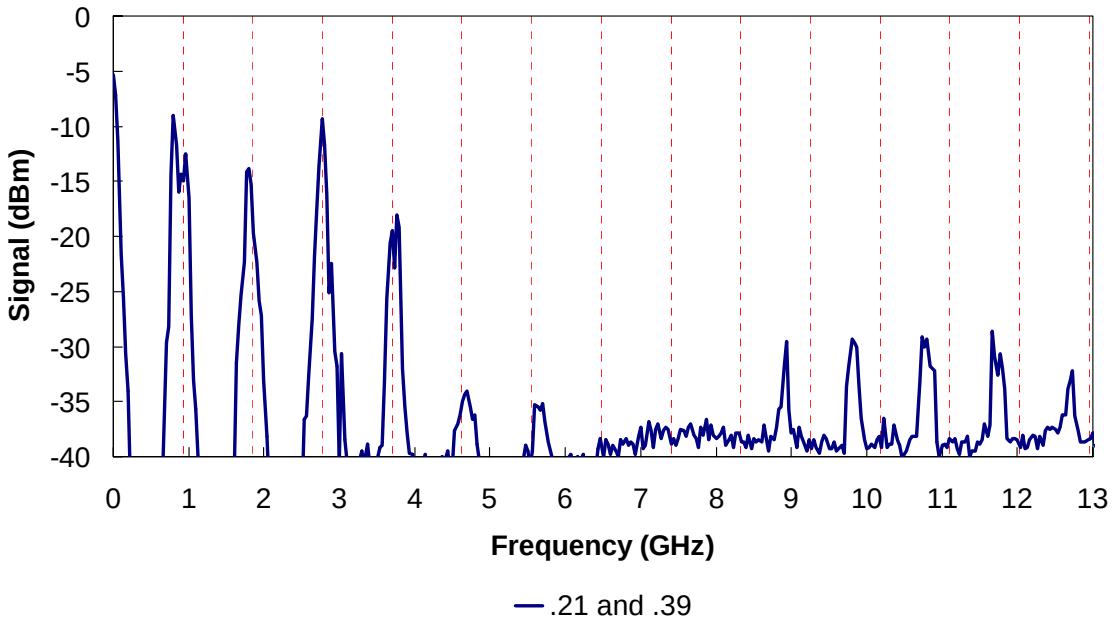

Figure 27. Power spectrum of the output corresponding to the optical spectrum of Figure 26. The red lines are at 0.93 GHz and its harmonics. Note that the peaks centered around 10.7 GHz are not harmonics of the lower frequency sequence of peaks though they have the same spacing. The center one is at the 10.7 GHz Brillouin scattering frequency.

spectrum between 9-13 GHz result from the beating between the central peak and the offset peak. Note that one of these four peaks has an offset at 10.7 GHz, matching the expected offset

for Brillouin scattering. Therefore, we can associate the offset feature with SBS. Also note that the spacing between the higher frequency peaks maintains the 0.93 GHz spacing of the lower frequency peaks but that these peaks are not at harmonics of this frequency. They are offset to match the Brillouin shift, which typically is < 100 MHz. Because the Brillouin shift moves the feature outside of the simultaneous high reflection band, there is a relatively weaker constraint on the modes imposed by the length mismatch. Effectively, only one of the two amplifier paths has the high roundtrip gain. Therefore the SBS can be established independent of the path length mismatch. Because, the optical nonlinearity due to the acoustic interaction has a fairly small bandwidth, the gain at the Brillouin shift becomes the dominant force in pulling these modes back near or to the threshold oscillation condition.

We observe other evidence of competition between SBS and XMC as the length mismatch was reduced between the two lasers. The spectral features, i.e. the mode clusters but not the individual modes, broadened. When the length mismatch was less than about 4 cm so that the 10.7 GHz SBS frequency was near the third harmonic, we observed that the spectral feature was not centered on the SBS offset frequency. Figures 28 and 29 show examples of this, as do Figures 23 and 24 with the SBS frequency near the fourth harmonic. Previously, when we worked with four-laser configurations with broader high reflection spectral regions we would often observe that the spectral clusters near 10.7 GHz were weaker than those at higher frequencies. It appears that there is some complicated interplay between the SBS and XMC. We will try to perform additional experiments to understand this interplay in the next quarter. Unfortunately, this is where the parasitic etaloning effects became crucial for our interpretation of spectra. We could never separate the complex spectral patterns we observed, and the time dependent fluctuations, from the possibility of intracavity etalon effects.

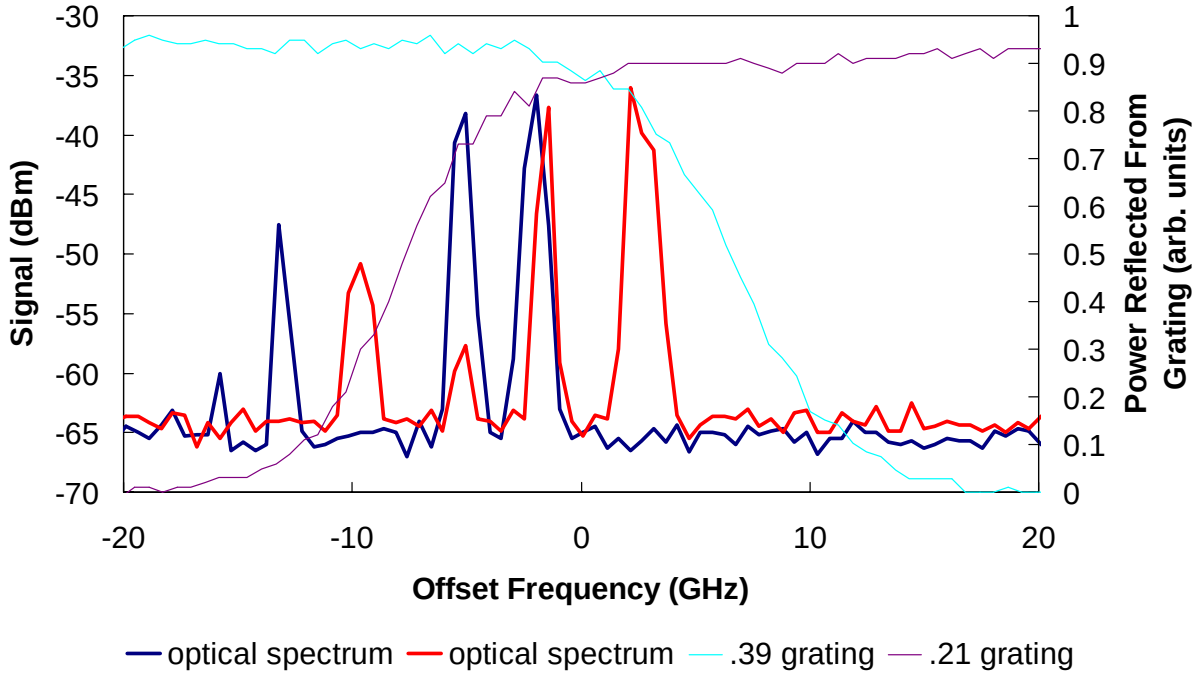

Figure 28. Optical spectra showing taken at different times using the same configuration. The SBS peak is approximately at a multiple of the XMC broadened peaks.

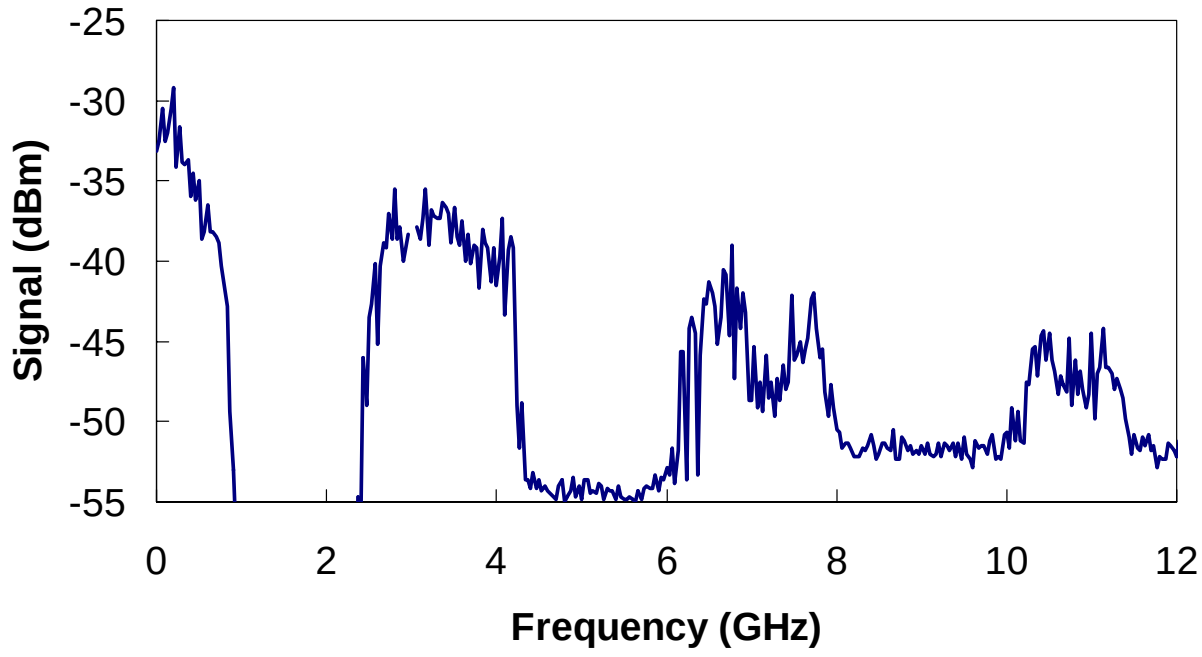

Figure 29. Power spectrum to go with Figure 28. Unlike the previous power spectra this was taken using the max hold setting so is an average of several traces. The 10.7 GHz Brillouin shift is within the highest frequency broad feature but is not at the center.

7.0 RELAXATION PULSATION PHENOMENA

When parasitic etaloning effects forced us to abandon our investigation of whether the spectra of the coherently coupled arrays could show erratic variations due to deterministic origins or only to stochastic ones, we returned to a topic that we briefly investigated earlier. Fiber lasers, and similar solid-state lasers are known to have a range of bias points where they operate in a self-pulsing mode. This self-pulsing mode is to be distinguished from fluctuations due to random longitudinal mode phasing by the time scale, typically tens to hundreds of microseconds rather than the sub-microsecond scale of the multimode temporal fluctuations. The period for these pulsations is determined by the relaxation resonance condition, on the order of the geometric mean of the cavity photon lifetime and gain spontaneous decay rate. It is well known that as the laser pump power is increased above threshold that the laser that relaxation oscillations can be induced in solitary lasers and that the oscillation period decreases with increasing gain. Eventually, the relaxation pulsations are suppressed at sufficiently high gain levels. We believed that investigations of these phenomena would be less susceptible to the effects of intracavity etaloning because they were inherently pulsating in nature.

Using a two-laser array like that shown in Figures 1 and 2(a), we have previously observed that the pulsations can display a different behavior. If we excite one laser so that it is just pulsating and then turn on the second laser, we observe that the relaxation period increases rather than decreases as the gain of the second laser crosses threshold and enhances the pulsation. We investigated the two-laser array again, this time emphasizing operation where the high reflections in a round trip are limited to a small spectral range, as with the previous measurements that demonstrated the presence of SBS. Previously, the data had been taken with a larger high reflection spectral region.

Because we wanted to compare the single-laser and two-laser configurations, we did not reproduce the arrangement of Figure 1. Instead, we used the linear configurations shown in Figure 30. The two minimally overlapping FBGs are put at either end of a linear cavity. Light output is predominantly through a 90/10 fiber coupler/splitter. One or two amplifiers can be inserted, with the latter in a Mach-Zehnder configuration as shown in Figure 30(b). In the single amplifier configuration the laser either began pulsation at or within 1% of threshold. The range of pump levels where the pulsation occurred decreased with increasing cavity length, as shown

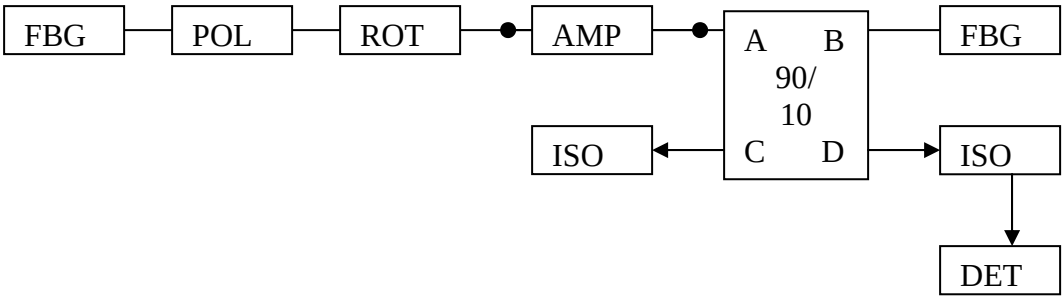

Figure 30(a)

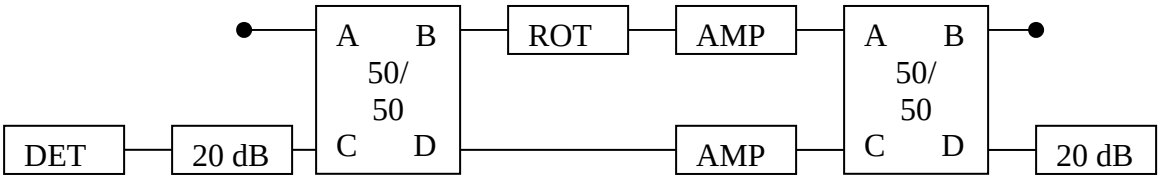

Figure 30(b)

Figure 30. Schematic of the new configuration used to test the relaxation oscillation phenomena. The FBGs are chosen to have minimal overlap. A single linear polarization is enforced by a fiber polarizer (labeled POL in the figure) and polarization rotating elements (ROT). Optical isolators (ISO) and 20 dB optical attenuators (20 dB) are used to isolate the cavity from external reflections. 100 mW Erbium-doped fiber amplifiers (AMP) provide gain. Various photodiodes (DET) are used to monitor the cavity. (a) Single amplifier configuration and (b) insert in place of single amplifier to convert to Mach-Zehnder two-amplifier configuration.

in Figure 31. Plotted in this figure are the lower bound, essentially threshold, of the pulsation region, upper bound, a power where the pulsation achieved the highest amplitude and shortest pulse width. Figure 32 shows how the pulsation frequency and pulse width varied with pump parameter. In the usual manner, the frequency varied with the square root of the pump parameter. The pulse width begins to broaden while the resonance frequency continues to decrease with increasing pump level, so that the pulsing makes a smooth transition to a more sinusoidal modulation on an increasing constant background before disappearing. Similarly, the pulse width narrows from a more sinusoidal modulation at levels just above threshold.

Interestingly, the laser always entered the pulsation regime smoothly as the current was raised above threshold with a frequency of ~ 4.8 kHz ±10%, regardless of cavity length. The frequency at the minimum pulse width, and the maximum frequency observed, scale approximately

inversely with cavity length while the minimum pulse width scales in proportion to the cavity length, as shown in Figure 33.

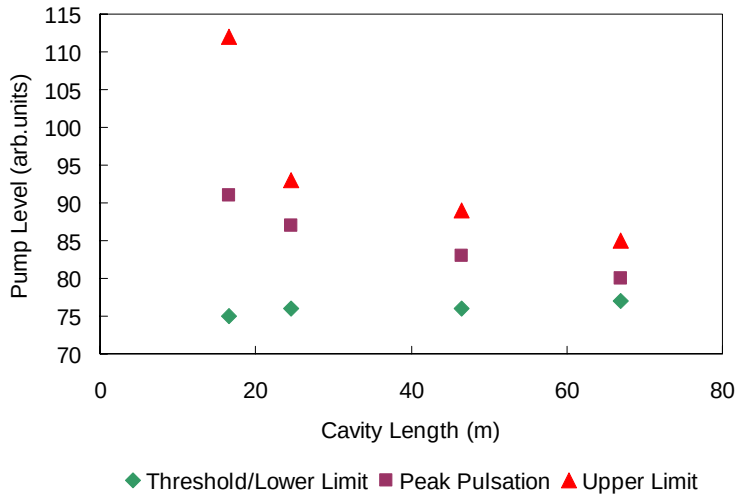

Figure 31. Plot of the range of relaxation oscillations as a function of cavity length for the cavity of Figure 30(a). The pump power level is proportional to the bias current to the pump laser diodes of the Er-doped fiber amplifiers. The laser entered the oscillation regime at or just above threshold. The peak pulsation is the power level where the pulse amplitude was a maximum and pulse width a minimum.

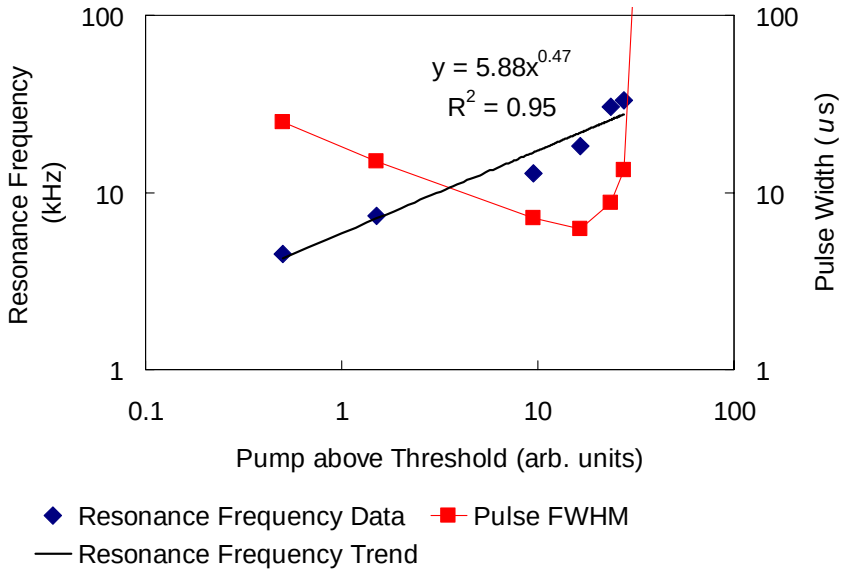

Figure 32. Variation of the resonance frequency and the pulse width as the pump level increases above threshold (a value of 74.5 using Figure 31). The baseline cavity configuration, ~16.6 m cavity length, was used. The equation is the least-squares fit to a power curve for the resonance frequency data.

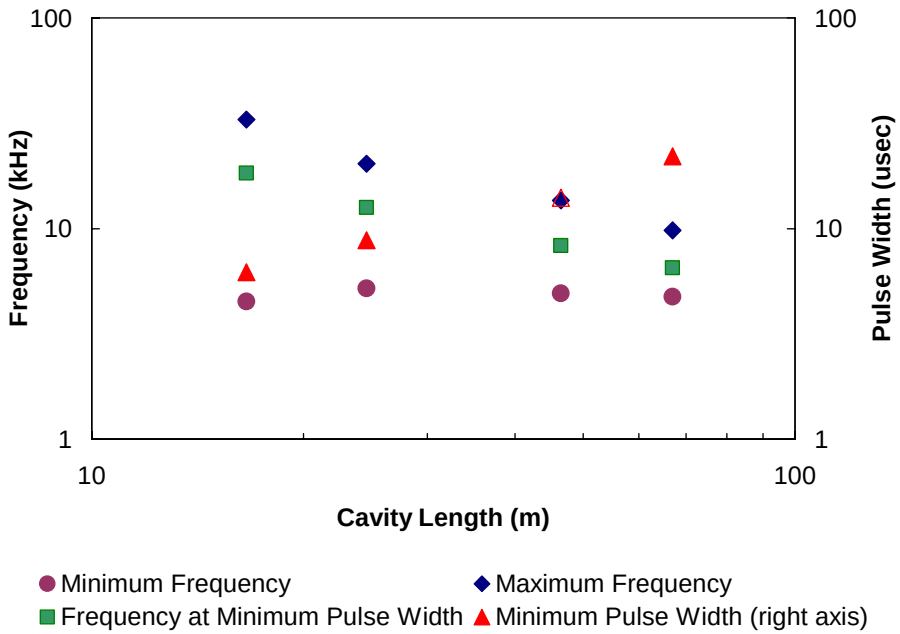

Figure 33. Variations in the minimum pulsation frequency observed just above threshold, the pulsation frequency observed at the minimum pulse width, the maximum frequency observed at the high pump edge of the pulsation range, and the minimum pulse width as a function of cavity length.

As we reported during the last phase of this effort, the situation becomes more complex when coherently coupled amplifiers are used. We qualitatively verified the previous observation that the resonance frequency could decrease with increasing pump levels with the configuration of Figure 31(b). This time we observed that for both the one- and two-amplifier configurations that increased losses within the cavity tended to reduce the range of pump levels where the pulsations were observed. However, the two sets of data showed that the increased pulsation period was consistent with the fact that the second laser was having an increasing effect on the pulsation period as its gain contributed more to the overall output. When it reached the same pump level as the first amplifier, the pulsation period was always decreasing and the output always stronger as summarized in Figure 34, data taken during the last contract. The pulsation period then appears to be due to a weighted average of the two coherent pathways and is subject to a greater degree of control than with an individual cavity. This may be a useful feature. We did not observe any effects due to the narrowing of the high reflection spectral band.

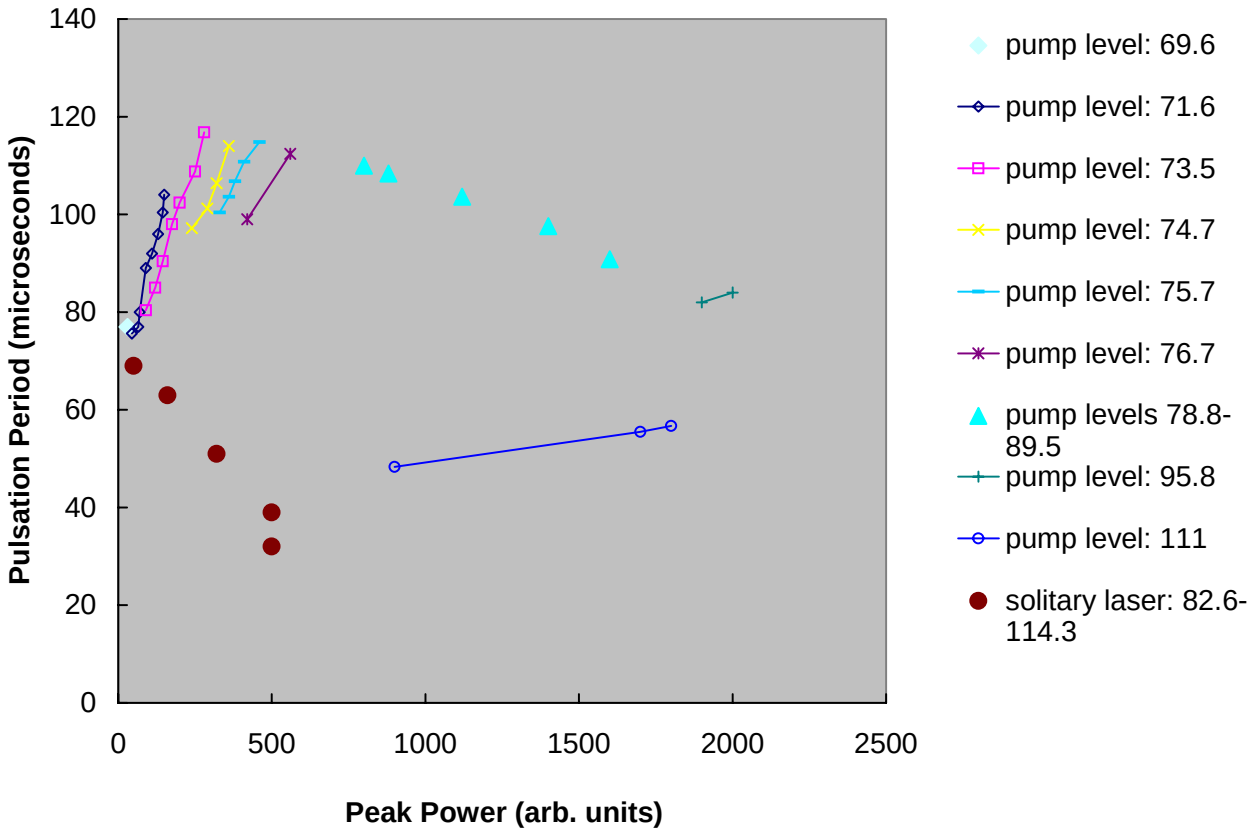

Figure 34. The pulsation period of the two-laser system as a function of the pulse power. One laser is biased at 132.4 where it displayed pulsating output of the combined cavity. The pump level to the large amplifier is varied over the range of pulsating output, with its output at a pump level of 80 equal to that of the first amplifier. Data points connected by lines were taken at the same pump level. Also shown, the brown circles are the data for the large amplifier as its pump level is varied and the other laser is unpumped.

8.0 DISCUSSION AND CONCLUSIONS

Before proceeding to a culminating interpretation of the experimental results, we want to emphasize that one of the conclusions of this effort is that it is impossible to use FC/APC connectors reliably in an intracavity configuration when single-mode laser powers approaching 1 W are present. Over time, even good connections can degrade and lead to the parasitic etalon effects. Even the relatively modest intracavity powers we generated, 1 W or less, are sufficient to cause problems with conventional fiber connectors. To be sure, 1 W in a single mode fiber is a high average intensity, on the order of a megawatt per square centimeter, and the peak powers could easily be orders of magnitude higher due to the random phasing of the various modes and pulsations in the output. We recommend fusion splices for all future work. Highly accurate fusion splicers for single-mode fibers are now manufactured commercially for use in the field by technicians. These portable devices cost $15-$20K.

Siegman has written an analysis of the linear coupling of lasers that is appropriate to the experimental configuration that we are investigating [4]. Considering only linear mechanisms, a key point of Prof. Siegman's analysis is the conclusion that the linear, interferrometric coupling mechanism that has worked for the coupling of arrays up to eight lasers becomes increasingly problematic for scaling much beyond this point. As we have pointed out, this requires that there be fortuitous degeneracies of the modes of the isolated lasers such that the modes of the compound array suffers little dephasing loss on a round trip in any of the multiple array arms. Prof. Siegman quantifies just how difficult this will be for arrays of 10 elements or larger. However, because this is only a linear analysis, it does not consider the mode coupling due to the fiber Kerr nonlinearity induced XMC. As we have demonstrated, this is the first nonlinearity that demonstrably modifies the output spectrum of the laser array by causing power to be coupled from stronger to weaker modes. This mechanism will greatly increase the number of available modes for coherent coupling in the array.

The SBS nonlinearity appears next as the power is increased and it appears to have a complex interaction with the XMC. With a two laser configuration, we observed that coherent coupling was lost when the path length difference between the lasers became sufficiently short so that the beat frequency exceeded ~ 10 GHz. This frequency was smaller than the 40-50 GHz high reflection band of the FBGs, and similar to the Brillouin shift. If the two laser amplifiers in the

coupled configuration had separate FBGs with a spectral overlap of ~ 10 GHz or less, then we observed an offset peak out of the narrow common high reflection band. This offset peak was always on the long wavelength side, near the 10.7 GHz offset expected for SBS. However, the peak offset was shifted from the precise SBS offset to match a multiple of the frequency shift enforced by the cavity length mismatch of the two elements of the array. Again, the SBS-shifted peak appeared at approximately the same circulating power levels as the spectral broadening appeared within band. Because the XMC appears to dominate within band and there appears to be reduction rather than enhancement of features at offset frequencies around 10.7 GHz when they would be within the high reflection band, our results tentatively indicate that the interaction of SDBS and XMC is negative for the coherent coupling application. As the number of mode clusters within the high reflection bandwidth was reduced, we stopped being able to observe clean output spectra unless the 10.7 GHz SBS offset was reasonably well matched with a harmonic of the coupled cavity length mismatch. Unfortunately, our results were complicated by the parasitic etaloning and further work will be necessary to fully clarify this point.

We have also become aware of a set of papers investigating the Kerr nonlinearity as a passive mode-locking mechanism [10]. These papers identify the kind of XMC that we are using in long fiber lasers as a mechanism to induce mode locking and high repetition rate, short pulse (dark pulse under conditions of normal dispersion as is the case in our experiments) generation. The papers are not clear on this issue but they do not seem to observe the spectral broadening that we observe in our cavities. The coupled cavities in our arrays are a natural mechanism to modulate the losses as a function of optical frequency and induce coherent coupling. However, mode locking requires more than just coherent coupling and, to date, we have not observed the kind of mode locking that would lead to short pulse generation.

Therefore, it would appear that there might be an optimal or multiple optimal cavity lengths to induce the appropriate nonlinearity based on the type of output to be generated. For high average power applications, pulse formation, except for dark pulse formation, should probably be discouraged as it could lead to catastrophic material damage. In this case, the coherent coupling and spectral spreading observed in our cavities might be ideal if it can be accomplished with no mode locking. Also, a cavity of appropriate length needs to be chosen to minimize polarization scrambling.

Single-fiber power levels are already approaching the intrinsic limits [1]. Therefore, a coherently coupled multi-core configuration, such as has been analyzed by several groups [11,12], is a more likely ultimate configuration. The multicore configurations use nearest-neighbor coupling rather than the global coupling scheme of our past work. However, we believe that there is no compelling evidence at this time to indicate that the global coupling will produce insight into the onset of the nonlinear optical effects that is not relevant to the nearest-neighbor schemes. Certainly, if the nearest-neighbor coupling region is sufficiently long and the nonlinear interactions sufficiently small, there will be effective global coupling over the nonlinear interaction length.

One group has postulated that there is an intrinsic nonlinearity in the intracavity coupled array configuration that is not apparent linearized modal analysis [13] and that this nonlinearity is significant and will lead to dynamics not anticipated by the linearized analysis. For instance, they assert that the self-organized coherence cannot be explained by a calculation of the linearized fully-coupled array modes which show that the dominant round-trip gain (or minimal loss) is restricted to those array modes that are simultaneously near-degenerate with a mode of each of the individual laser cavities. This is at variance with the findings of another group [3] where the scaling of coherent power with number of laser (up to eight) is consistent with the modal analysis. We also see no evidence of an emergent nonlinearity in our studies as the complexity of the array is increased. Therefore, we believe that one must rely on the intrinsic fiber material nonlinearities, XMC and SBS that we have observed, to overcome the limits on array scaling imposed by the linearized modal analysis. However, and this is one of the key unanswered questions from the current research, we have been unable to rule out novel nonlinear interactions based on the dynamics and complexity of the coherently coupled arrays, particularly when high-reflection bandwidth and fiber length mismatch lead to situations where there are no allowed high gain modes in the linear analysis. We observed fluctuations in the spectral characteristics of arrays of more than four elements that we have attributed to the influence of parasitic etaloning due to microdamage. However, the etaloning may have been masking an intrinsic nonlinear limitation.

9.0 RECOMMENDATIONS FOR FUTURE WORK

To continue these investigations, we would propose to experimentally investigate combining the observed coherent self-organization capabilities of small numbers of fibers, spectral spreading due to XMC and active phase control in a fiber laser array as a means to achieve very high powers in a multi-element array. We believe that the active phase control can be used to optimize the intracavity coupled array. Because active phase control of each element in a massive array is prohibitively complex, we would rely on the self-organization and XMC effects to perform the output optimization at the individual laser level, and that the active phase control can be used to maintain coherence between sub-elements of the array that could drift in and out of coherence due to environmental effects and length mismatch.

Such a program would continue to emphasize experimental measurements using commercially available components of modest power. To observe nonlinear optical effects we will configure the lasers in very long optical cavities. Nonlinear optical effects such as XMC and SBS scale as a function of the product of the power and cavity length. The use of long cavities has the added benefit of reducing the intrinsic relaxation resonance frequency of the fiber lasers. This is helpful because newly available commercial components can be used to actively control the phase of the circulating laser field at modulation frequencies above the long cavity relaxation resonance frequency. This will allow control of the cavity and permit investigation of key parameters related to the onset of nonlinear optical effects in the coherently coupled array. Understanding this onset is critical in the scaling of fiber lasers to very high power levels.

Such work would require the elimination of intracavity parasitic reflections through the use of fusion-spliced fibers. By minimizing the intracavity parasitics, one would be able to unambiguously relate the spectral characteristics to the intrinsic properties of the intracavity coupled system. By controlling the optical phase, precise positioning of high-gain array modes within the high-reflection bandwidth region of FBGs is facilitated. This allows considerable control and flexibility of the array configuration for control of cavity gain and gain bandwidth.

A step-by-step approach would first concentrate on a two laser array, in part because it is the simplest to compare to models of the laser array. We have already observed the onset of the spectral broadening due to XMC and the appearance of SBS in a two-laser array. The elimination of the parasitic reflections and the ability to actively control the optical phase of the intracavity

laser field will allow a more precise study the onset of these nonlinear optical interactions and their effect on the coherence of the circulating optical field. The fusion splicing technology will allow control of path length differences to the centimeter level. Combined with new commercially available components, this will permit active control of the phase length of the laser path enabling more precise determination of key parameters.

The two lowest power optical nonlinearities that we have observed, XMC and SBS, have very different interaction bandwidths. The former is very broadband while the later has a relatively narrow bandwidth. Therefore, we anticipate that the onset of these two nonlinearities should depend strongly on the spectral characteristics of the circulating laser field. The higher the concentration of power into a discrete spectral region or regions, the lower the threshold for the SBS relative to the XMC. Therefore, a first extension from the two-laser array would be to an asymmetric four-laser array. Each arm of the strong amplifier (0.5 W saturation power) two-laser array will be augmented by a low-power amplifier (0.1 W saturation power) in a parallel Mach-Zehnder arm. The purpose of this length mismatched arm will be to concentrate the optical power into a smaller number of modes. By adjusting the length mismatch and actively controlling the phase length we anticipate that we will see very different onset characteristics for the two nonlinear mechanisms. This will be strong confirmation that we have identified the key elements of the underlying physics.

Next in complexity would be to reconfigure the array into an asymmetric five-laser configuration with a single 0.5 W amplifier arm coupled to a four-laser array of 100 mW amplifier arms. This configuration has shown the greatest spectral irreproducibility in our ongoing work, irreproducibility that may be due to intracavity parasitic reflectances, but may also be due to intrinsic nonlinear optical effects as have been predicted by others [13]. By changing the cavity length mismatches and actively controlling the phase of a subset of the five amplifiers, we will be able to investigate the stability characteristics of the configuration and map out domains of intrinsic nonlinear dynamics. We emphasize that our experimental approach provides a degree of flexibility and control not shared by other groups and our use of long cavities allows investigation of nonlinear optical interactions with this control using relatively low power systems. By using ar long cavity length configuration and active phase control, quantitative investigations of the countering mechanisms of spectral narrowing due to length mismatch and broadening due to the nonlinear optical interactions can be performed. This will yield key

information for scaling to large arrays using nonlinear optical interactions augmented by active phase control in intracavity coupled fiber laser arrays.

Such an effort would fill an important gap in the current understanding of coherently coupled arrays, the effects of fiber nonlinearities on active phase control and spontaneous self-organization. To date, with the exception of our work, all ongoing work on coherent coupling of fiber arrays has worked in regions that minimize fiber nonlinearities. However, because the output of individual fibers is now pushing into the domain of significant nonlinear interactions, it is critical that the effects of these nonlinearities on coherent coupling be understood. This is true for both global and nearest-neighbor coupling configurations.

10.0 REFERENCES

[1] A. Tünnermann, T. Schreiber, F. Röser, A. Liem, S. Höfer, H. Zellmer, S. Nolte, and J. Limpert, "The renaissance and bright future of fibre lasers," *J. Phys. B, At. Mol. Opt. Phys.*, **38**, S681 (2005).

[2] Y. Jeong, J.K. Sahu, M. Laroche, W.A. Clarkson, K. Furusawa, D.J. Richardson, and J. Nilsson, 2003 Conference on Lasers and Electro-Optics Europe, 626 (2003)).

[3] A. Shirakawa, K. Matsuo, and K. Ueda, "Fiber laser coherent array for power scaling, bandwidth narrowing, and coherent beam direction control, *Proc. SPIE* **5709**, 165 (2005).

[4] A. E. Siegman, "Resonant modes of linearly coupled multiple fiberlaser structures," submitted to *J. Opt. Soc. Am.*

[5] T.B. Simpson, "Fiber Laser Array," *AFRL-DE-PS-TR-2004-1028*, (2004).

[6] T.B. Simpson, A. Gavrielides, and P. Peterson, "Coherent Intra-cavity Coupling of Fiber Lasers," *Proc. 14th Annual Mtng. IEEE LEOS*, 62 (2001).

[7] T.B. Simpson, A. Gavrielides, and P. Peterson, *Optics Express* **10**, 1060 (2002).

[8] See, for example, General Photonics Corp. FPS-001 Fiber Phase Shifter, www.generalphotonics.com.

[9] T.B. Simpson, "Fiber Laser Array," *AFRL-DE-TR-2001-1090*, (2002).

[10] M. Quiroga-Teixeiro, et al., "Passive Mode Locking by Dissipative Four-Wave Mixing," *Journal of the Optical Society of America*, Part B **15**, 1315 (1998), T. Sylvestre, et al., "Self-Induced Modulational Instability Laser Revisited: Normal Dispersion and Dark-Pulse Train Generation," *Optics Letters* **27**, 482 (2002).

[11] P.K. Cheo, A. Liu, and G.G. King, "A High-Brightness Laser Beam From a Phase-Locked Multicore Yb-Doped Fiber Laser Array," *IEEE Photonics Technology Letters* **13**, 439 (2001), E. J. Bochove, P. K. Cheo, and G. G. King, "Self-organization in a multicore fiber laser array," *Optics Letters* **28**, 1200 (2003).

[12] S. Peles, J. L. Rogers, K. Wiesenfeld, "Synchronization in fiber laser arrays: theoretical study," *Proceedings of the SPIE* **5971**, 190 (2005).

[13] H. Bruesselbach, D.C. Jones, M.S. Mangir, M. Mi nden, and J.L. Rogers, “Self-organized coherence in fiber laser arrays,” *Opt. Lett.* **30**, 1339 (2005).

DISTRIBUTION LIST

DTIC/OCP
8725 John J. Kingman Rd, Suite 0944
Ft Belvoir, VA 22060-6218 1 cy

AFRL/VSIL
Kirtland AFB, NM 87117-5776 2 cys

AFRL/VSIH
Kirtland AFB, NM 87117-5776 1 cy

Official Record Copy
AFRL/DELO/Dr. Peterson 2 cy

L-3 Communications-Jaycor
Attn: Tom Simpson
3394 Carmel Mountain Road
San Diego, CA
92121 2 cy

This page is intentionally left blank.